

Bipartite Mixed Membership Distribution-Free Model. A novel model for community detection in overlapping bipartite weighted networks

Huan Qing^{a,*}, Jingli Wang^b

^a*School of Mathematics, China University of Mining and Technology, Xuzhou, 221116, Jiangsu, China*

^b*School of Statistics and Data Science, KLMDASR, LEBPS, and LPMC, Nankai University, Tianjin, 300071, Tianjin, China*

Abstract

Modeling and estimating mixed memberships for overlapping unipartite un-weighted networks has been well studied in recent years. However, to our knowledge, there is no model for a more general case, the overlapping bipartite weighted networks. To close this gap, we introduce a novel model, the Bipartite Mixed Membership Distribution-Free (BiMMDF) model. Our model allows an adjacency matrix to follow any distribution as long as its expectation has a block structure related to node membership. In particular, BiMMDF can model overlapping bipartite signed networks and it is an extension of many previous models, including the popular mixed membership stochastic block models. An efficient algorithm with a theoretical guarantee of consistent estimation is applied to fit BiMMDF. We then obtain the separation conditions of BiMMDF for different distributions. Furthermore, we also consider missing edges for sparse networks. The advantage of BiMMDF is demonstrated in extensive synthetic networks and eight real-world networks.

Keywords: Community detection, complex networks, distribution-free model, overlapping bipartite weighted networks

1. Introduction

Complex networks are ubiquitous in our daily life (Dunne et al., 2002; Palla et al., 2007; Barabasi & Oltvai, 2004; Guimera & Nunes Amaral, 2005; Rubinov & Sporns, 2010). A network is composed of a set of nodes and edges which represent the relationship between nodes. Many real-world networks of interest may be described by bipartite graphs, and they are bipartite networks or two-mode networks (Borgatti & Everett, 1997; Latapy et al., 2008). In a bipartite network, nodes are decomposed into two disjoint sets such that edges can only connect nodes from different sets. Let us cite some bipartite networks for examples. In the actors-movies network (Watts & Strogatz, 1998; Latapy et al., 2008), each actor is linked to the movies he/she played in; in the author-paper network (Newman, 2001b,a), each author is linked to the paper he/she signed; in the country-language network Kunegis (2013), each country is linked to the language it hosts and edge weight denotes the proportion of the population of a given country speaking a given language; in the character-work network Alberich et al. (2002), each character is linked to the movie he/she appears in; in the user-movie network Guo et al. (2014), movies are rated by users; in the user-item network Wang et al. (2010), individual items are rated by users. More examples of bipartite networks can be found in Latapy et al. (2008). In the above bipartite networks, a node may belong to multiple clusters rather than a single cluster. For example, in the actors-movies network, Jackie Chan can be classified as an action & comedy actor and a movie like “Rush Hour” belongs to action and comedy. Such overlapping membership is common in real-world networks (Palla et al., 2005; Airoidi et al., 2008; Mao et al., 2020). This paper focuses on inferring each node’s community membership to have a better understanding of the community structure of overlapping bipartite weighted networks.

Community detection is one of the most powerful tools for learning the latent structure of complex networks. The main goal of community detection is to find group of nodes (Fortunato, 2010; Fortunato & Hric, 2016). To solve

*Corresponding author.

Email addresses: qinghuan@u.nus.edu (Huan Qing), jlwang@nankai.edu.cn (Jingli Wang)

the community detection problem, researchers usually follow three steps for model-based methods. In the first step, a null statistical model is used to generate networks with community structure (Goldenberg et al., 2010; Jin et al., 2021). In the second step, an algorithm is designed to fit the model and it is expected to infer communities satisfactorily for networks generated from the model. In the third step, the algorithm is applied to detect communities for real-world networks. For different types of networks, different statistical models should be proposed and so are the algorithms. Generally speaking, for static networks considered in this article, there are four cases: un-directed un-weighted networks, bipartite un-weighted networks, un-directed weighted networks, and bipartite weighted networks, where the first three cases are special cases of bipartite weighted networks. Note that directed networks Malliaros & Vazirgiannis (2013) can be regarded as a special case of bipartite networks since directed networks are unipartite or one-mode (Zhang & Wang, 2022; Rohe et al., 2016). To have a better knowledge of statistical models for these cases, we will briefly introduce several representative statistical models for each case.

For community detection of un-directed un-weighted networks, it has been widely studied for decades (Fortunato, 2010; Papadopoulos et al., 2012; Fortunato & Hric, 2016; Javed et al., 2018; Jin et al., 2021; Fortunato & Newman, 2022). The Stochastic Blockmodel (SBM) (Holland et al., 1983) is one of the most popular generative models to describe community structure for such networks. SBM assumes that the probability of a link between two nodes is determined by node communities. Though SBM is mathematically simple and easy to analyze, it performs poorly on real-world networks because it assumes that nodes in the same community have the same expected degree. The Degree-Corrected Stochastic Blockmodels (DCSBM) (Karrer & Newman, 2011) was proposed to address this limitation by considering the node heterogeneity parameters. To detect communities of networks generated from SBM and DCSBM, substantial works have been proposed in recent years, including maximizing the likelihood methods (Karrer & Newman, 2011; Bickel & Chen, 2009; Zhao et al., 2012), low-rank approximation method (Le et al., 2016), convexified modularity maximization method (Chen et al., 2018), and spectral clustering algorithms (Rohe et al., 2011; Jin, 2015; Lei & Rinaldo, 2015; Joseph & Yu, 2016). For a comprehensive review of recent developments about SBM, see Abbe (2017). One main limitation of SBM and DCSBM is that each node only belongs to a sole community. The classical Mixed Membership Stochastic Blockmodels (MMSB) (Airoldi et al., 2008) was proposed as an extension of SBM by allowing nodes to belong to multiple communities. The Degree-Corrected Mixed Membership (DCMM) model (Jin et al., 2023) extends DCSBM from non-overlapping networks to overlapping networks. The Overlapping Continuous Community Assignment Model (OCCAM) (Zhang et al., 2020), the Stochastic Blockmodel with Overlaps (SBMO) (Kaufmann et al., 2018), and the Overlapping Stochastic Block Models (OSBM) (Latouche et al., 2011) can also model overlapping networks. To estimate mixed memberships of networks generated from MMSB and DCMM, some methods are proposed, including MCMC (Airoldi et al., 2008), variational approximation method (Gopalan & Blei, 2013), nonnegative matrix factorization inference methods (Ball et al., 2011; Psorakis et al., 2011; Wang et al., 2011), tensor-based method (Anandkumar et al., 2013), and spectral methods (Jin et al., 2023; Mao et al., 2018; Zhang et al., 2020; Mao et al., 2020). For a general review on overlapping community detection, see Xie et al. (2013).

For community detection of bipartite un-weighted networks, Rohe et al. (2016) proposed Stochastic co-Blockmodel (ScBM) and Degree-Corrected Stochastic co-Blockmodel (DCScBM). ScBM and DCScBM can be seen as direct extensions of SBM and DCSBM from un-directed un-weighted networks to bipartite un-weighted networks, respectively. Spectral algorithms with theoretical guarantees on consistent estimation have been designed to estimate groups of nodes under ScBM and DCScBM, see algorithms proposed in Rohe et al. (2016); Zhou & Amini (2019); Wang et al. (2020). Similar to SBM, ScBM also can not model overlapping networks. The Directed Mixed Membership Stochastic Blockmodels (DiMMSB) (Qing & Wang, 2021) was proposed to address this limitation by allowing nodes to belong to multiple communities. DiMMSB can be seen as a direct extension of MMSB from un-directed un-weighted networks to bipartite un-weighted networks. To estimate memberships under DiMMSB, Qing & Wang (2021) designed a spectral algorithm with a theoretical guarantee of estimation consistency.

For community detection of un-directed weighted networks, it has been an appealing topic in recent years. Edge weights are important and meaningful in a network since they can improve community detection (Newman, 2004; Barrat et al., 2004). Newman (2004) studied a weighted network in which edge weights are nonnegative integers. To study a weighted network in which edge weights are more than nonnegative integers, many models extend SBM from un-directed un-weighted networks to un-directed weighted networks. Some Weighted Stochastic Blockmodels (WSBM) are developed in recent years (Aicher et al., 2015; Ahn et al., 2018; Palowitch et al., 2017; Xu et al., 2020; Ng & Murphy, 2021). However, these WSBMs always assume that each node only belongs to one single commu-

nity. To model overlapping un-directed weighted networks, the Weighted version of the MMSB (WMMSB) model (Dulac et al., 2020) was proposed as an extension of MMSB by allowing edge weights to come from Poisson distribution.

For community detection of bipartite weighted networks, the Bipartite Distribution-Free models (BiDFM) and its extension BiDCDFM were proposed by Qing & Wang (2023) to model non-overlapping bipartite weighted networks. The two-way blockmodels (Airolidi et al., 2013) can model overlapping bipartite weighted networks. However, one main limitation of the two-way blockmodels is that edge weights are limited to follow Normal or Bernoulli distribution which causes the two-way blockmodels can not to model some real-world bipartite weighted networks. For example, in the country-language network (Kunegis, 2013), edge weight ranges in $[0, 1]$; in the user-movie network (Guo et al., 2014) and user-item network (Wang et al., 2010), edge weight ranges in $\{0, 1, 2, 3, 4, 5\}$; in a bipartite signed network, edge weights ranges in $\{0, 1, -1\}$ (Tang et al., 2016). Such edge weights can not be generated from Normal or Bernoulli distributions. All aforementioned models fail to handle overlapping bipartite weighted networks in which edge weights can be any finite value and nodes can belong to multiple communities. Meanwhile, though the variational expectation-maximization (vEM) algorithm (Airolidi et al., 2013) was proposed to estimate community memberships for overlapping bipartite networks generated from the two-way blockmodels, it does not have any guarantees of consistency. In this article, our goal is to close these gaps and build a general model with a theoretical guarantee for overlapping bipartite weighted networks.

Our main contributions are summarized as follows:

- a) We propose a novel model for overlapping bipartite weighted networks, the Bipartite Mixed Membership Distribution-Free (BiMMDF for short) model. BiMMDF allows elements of the adjacency matrix to follow any distribution as long as the expectation adjacency matrix has a block structure. MMSB and the two-way blockmodels are sub-models of BiMMDF. Overlapping bipartite signed networks can also be modeled by BiMMDF. To the best of our knowledge, our BiMMDF is the first model for overlapping bipartite weighted networks in which edge weights can be generated from any distribution.
- b) We use an efficient spectral algorithm to estimate node memberships for overlapping bipartite weighted networks generated from BiMMDF. Theoretically, we show that the algorithm is asymptotically consistent under BiMMDF. We also derive the separation conditions of BiMMDF for different distributions. To our knowledge, we are the first to reveal the difference in separation conditions for different distributions.
- c) To model real-world large-scale bipartite weighted networks in which many nodes have no connections, we propose a strategy by combining BiMMDF with a model for bipartite un-weighted networks to generate adjacency matrices with missing edges.
- d) We conduct substantial simulated networks to verify our theoretical results. Our experiments on eight real-world networks demonstrate the effectiveness of our model in detecting and understanding community structure.

The rest of the paper is organized as follows. Section 2 introduces the model. Section 3 introduces the algorithm. Section 4 shows the consistency of the algorithm and provides some examples for different distributions. Section 5 introduces the strategy to generate missing edges. Section 6 conducts extensive experiments. Section 7 concludes.

2. The Bipartite Mixed Membership Distribution-Free model

The main symbols involved in this paper are summarized in Table 1. Given a bipartite weighted network $\mathcal{N} = (\mathcal{V}_r, \mathcal{V}_c, \mathcal{W})$ with n_r row nodes and n_c column nodes, where $\mathcal{V}_r = \{1, 2, \dots, n_r\}$ is the set of row nodes, $\mathcal{V}_c = \{1, 2, \dots, n_c\}$ is the set of column nodes, and \mathcal{W} represents the set of edge weights. Let $A \in \mathbb{R}^{n_r \times n_c}$ be \mathcal{N} 's bi-adjacency matrix. In this paper, we allow $\mathcal{V}_r \neq \mathcal{V}_c$, i.e., row nodes can be different from column nodes and a bipartite setting case. We also allow $A(i, j)$ to be any finite real values for $i \in [n_r], j \in [n_c]$ instead of only nonnegative values. For convenience, we call \mathcal{N} directed weighted network when $\mathcal{V}_r = \mathcal{V}_c$ (i.e., row nodes are the same as column nodes).

For an overlapping bipartite weighted network \mathcal{N} , our Bipartite Mixed Membership Distribution-Free model proposed in Definition 1 can model such \mathcal{N} .

Symbol	Description	Symbol	Description
\mathbb{N}	Set of nonnegative integers	\mathbb{N}_+	Set of positive integers
\mathbb{R}	Set of real numbers	\mathbb{R}_+	Set of nonnegative real numbers
\mathcal{N}	Bipartite weighted network	\mathcal{V}_r	Set of row nodes
\mathcal{V}_c	Set of column nodes	$P \in \mathbb{R}^{K \times K}$	Block matrix
K	Number of row (column) communities	$\ x\ _q$	ℓ_q -norm for vector x
n_r	Number of row nodes	M'	Transpose of matrix M
n_c	Number of column nodes	$\mathbb{E}[M]$	Expectation of M
$A \in \mathbb{R}^{n_r \times n_c}$	\mathcal{N} 's adjacency matrix	$\ M\ _{2 \rightarrow \infty}$	Maximum ℓ_2 -norm of M
$\Pi_r \in [0, 1]^{n_r \times K}$	Membership matrix of row nodes	$M(i, :)$	i -th row of M
$\Pi_c \in [0, 1]^{n_c \times K}$	Membership matrix of column nodes	$M(:, j)$	j -th column of M
$[m]$	$\{1, 2, \dots, m\}$ for positive integer m	$M(S_r, :)$	Rows in the index set S_r of M
ρ	Scaling parameter	$\text{rank}(M)$	Rank of M
$\sigma_k(M)$	k -th largest singular value of M	$\lambda_k(M)$	M 's k -th largest eigenvalue in magnitude
\mathcal{F}	Distribution	\mathcal{W}	Set of edge weights
$\Omega \in \mathbb{R}^{n_r \times n_c}$	A 's expectation matrix $\rho \Pi_r P \Pi_c'$	$\kappa(M)$	Condition number of M
$U \in \mathbb{R}^{n_r \times K}$	Top K left singular vectors of Ω	$\mathcal{P}_r \in \{0, 1\}^{K \times K}$	Permutation matrix
$V \in \mathbb{R}^{n_c \times K}$	Top K right singular vectors of Ω	$\mathcal{P}_c \in \{0, 1\}^{K \times K}$	Permutation matrix
$\hat{U} \in \mathbb{R}^{n_r \times K}$	Top K left singular vectors of A	$ a $	Absolute value for real value a
$\hat{V} \in \mathbb{R}^{n_c \times K}$	Top K right singular vectors of A	e_i	$e_i(j) = 1 (i = j)$
$\Lambda \in \mathbb{R}_+^{K \times K}$	Diagonal matrix of top K singular values of Ω	α_{in}	$\rho P(1, 1) = \alpha_{\text{in}} \frac{\log(n_r)}{n_r}$ when $K \geq 2$
$\hat{\Lambda} \in \mathbb{R}_+^{K \times K}$	Diagonal matrix of top K singular values of A	α_{out}	$\rho P(1, 2) = \alpha_{\text{out}} \frac{\log(n_r)}{n_r}$ when $K \geq 2$
$\hat{\Pi}_r \in [0, 1]^{n_r \times K}$	Estimated membership of row nodes	$\hat{\Pi}_c \in [0, 1]^{n_c \times K}$	Estimated membership of column nodes
τ	$\max_{i \in [n_r], j \in [n_c]} A(i, j) - \Omega(i, j) $	γ	$\max_{i \in [n_r], j \in [n_c]} \mathbb{E}((A(i, j) - \Omega(i, j))^2) / \rho$
$\text{diag}(M)$	Diagonal matrix with (i, i) -th entry $M(i, i)$	$\max(0, M)$	Matrix with (i, j) -th entry $\max(0, M(i, j))$
M^{-1}	Inverse of matrix M	I	Identity matrix of compatible dimension
p	Sparsity parameter	\mathcal{M}	Model for bipartite unweighted networks
η_r	Proportion of highly mixed row nodes	η_c	Proportion of highly mixed column nodes
ζ_r	Proportion of highly pure row nodes	ζ_c	Proportion of highly pure column nodes

Table 1: Main symbols of the paper.

Definition 1. Let $\Pi_r \in \mathbb{R}^{n_r \times K}, \Pi_c \in \mathbb{R}^{n_c \times K}$ such that $\text{rank}(\Pi_r) = K, \text{rank}(\Pi_c) = K, \Pi_r(i, k) \geq 0, \Pi_c(j, k) \geq 0, \|\Pi_r(i, :)\|_1 = 1$, and $\|\Pi_c(j, :)\|_1 = 1$ for $i \in [n_r], j \in [n_c], k \in [K]$, where $\Pi_r(i, :) \in \mathbb{R}^{K \times 1}$ and $\Pi_c(j, :) \in \mathbb{R}^{K \times 1}$ are the community membership vector for row node i and column node j , respectively. Let $P \in \mathbb{R}^{K \times K}$ satisfy $\max_{k, l \in [K]} |P(k, l)| = 1$ and $\text{rank}(P) = K$. Let $\rho > 0$ and call it the scaling parameter. Let $A \in \mathbb{R}^{n_r \times n_c}$ be the bi-adjacency matrix of \mathcal{N} . For all pairs of (i, j) , our Bipartite Mixed Membership Distribution-Free (BiMMDF) model assumes that for any distribution \mathcal{F} , $A(i, j)$ are independent random variables generated from the distribution \mathcal{F} satisfying

$$\mathbb{E}[A(i, j)] = \Omega(i, j), \text{ where } \Omega := \rho \Pi_r P \Pi_c'. \quad (1)$$

For convenience, denote our model by $\text{BiMMDF}(n_r, n_c, K, P, \rho, \Pi_r, \Pi_c, \mathcal{F})$. Figure 1 summarizes sketches of different types of overlapping networks modeled by our BiMMDF.

Remark 1. This remark provides some explanations and understandings on $K, \Pi_r, \Pi_c, P, \rho, \Omega$, and distribution \mathcal{F} under our model $\text{BiMMDF}(n_r, n_c, K, P, \rho, \Pi_r, \Pi_c, \mathcal{F})$.

- For K , it is the number of row (and column) communities and it is much smaller than $\min(n_r, n_c)$. When modeling a bipartite network in which both row and column nodes can belong to multiple communities, to make the model identifiable, the number of row communities must be the same as the number of column communities.
- For Π_r , it is the membership matrix for all row nodes. $\Pi_r(i, k)$ denotes the weight (which can also be seen as probability) of row node i on row community k for $i \in [n_r]$ and $k \in [K]$. The probability of row node i belonging to all the K row communities is 1, so BiMMDF requires $\sum_{k=1}^K \Pi_r(i, k) = 1$ for $i \in [n_r]$. Meanwhile, we require the rank of Π_r to be K because we need to make BiMMDF identifiable. Similar explanations hold for Π_c .
- For P , it controls the block structure of Ω to make BiMMDF more applicable. Otherwise, if P is an identity matrix, we have $\mathbb{E}[A(i, j)] = \Omega(i, j) = \rho \Pi_r(i, :) \Pi_c'(j, :)$, which is much simpler than $\rho \Pi_r(i, :) P \Pi_c'(j, :)$. Meanwhile, ρP in BiMMDF is not a probability matrix unless \mathcal{F} is Bernoulli distribution, and whether P can have

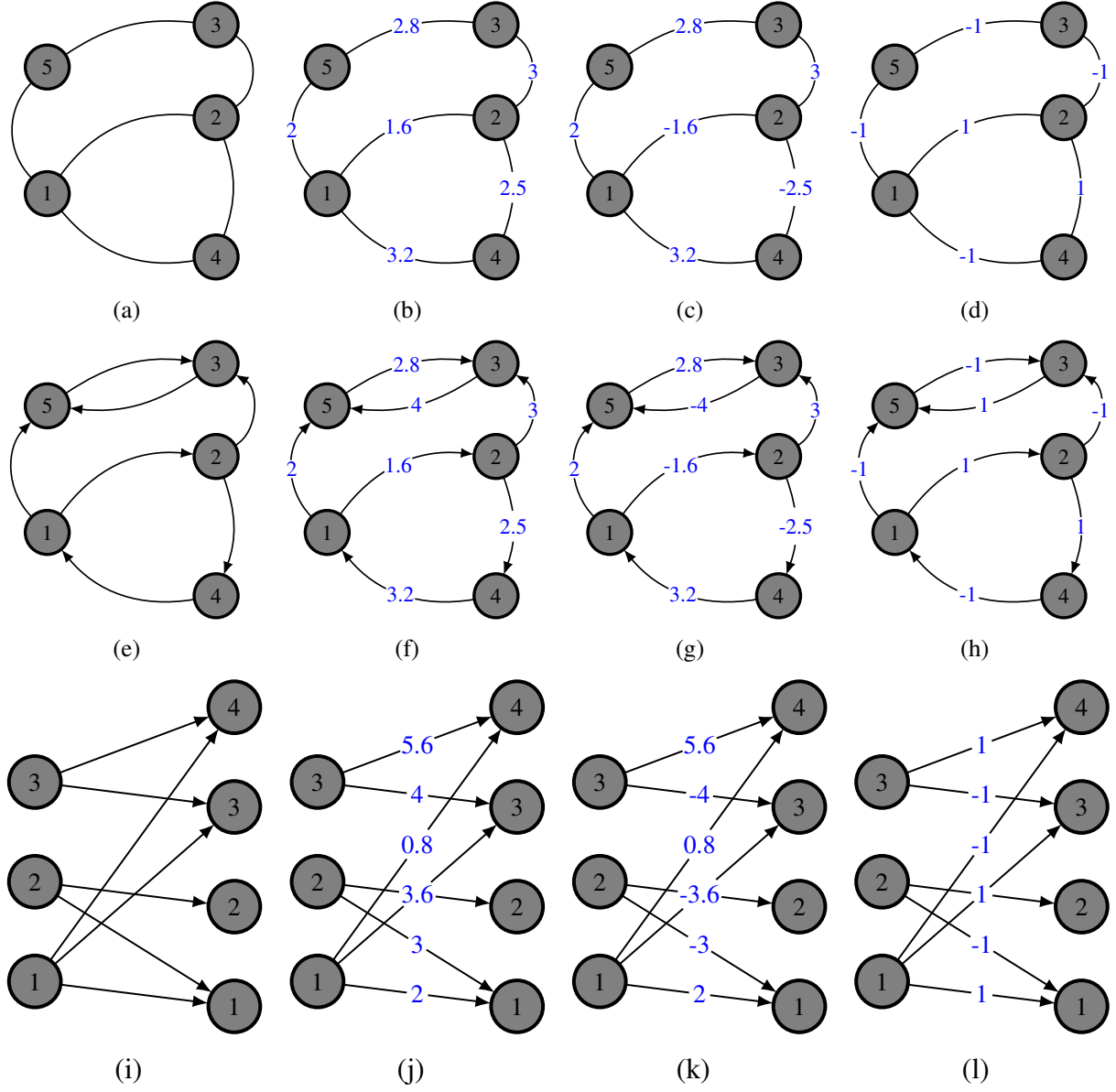


Figure 1: Illustrations for networks modeled by BiMMDF. Panel (a): un-directed un-weighted network. Panel (b): un-directed weighted network with positive weights. Panel (c): un-directed weighted network with positive and negative weights. Panel (d): un-directed signed network. Panel (e): directed un-weighted network. Panel (f): directed weighted network with positive weights. Panel (g): directed weighted network with positive and negative weights. Panel (h): directed signed network. Panel (i): bipartite un-weighted network. Panel (j): bipartite weighted network with positive weights. Panel (k): bipartite weighted network with positive and negative weights. Panel (l): bipartite signed network.

negative elements depends on distribution \mathcal{F} . For detail, see Examples 1-8. We set P 's maximum absolute element as 1 mainly for theoretical convenience because we have considered the scaling parameter ρ to make $\max_{k,l \in [K]} |\rho P(k, l)|$ be ρ . P is an asymmetric matrix, so BiMMDF can model bipartite networks (sure, P can be symmetric). Furthermore, we need P to be full rank to make BiMMDF well-defined and identifiable. For models like MMSB, OCCAM, DCMM, DiMMSB, and MMDF for overlapping networks, their identifiability also requires P to be full rank.

- For ρ , its range depends on distribution \mathcal{F} . For example, when \mathcal{F} is Bernoulli distribution such that ρP is a probability matrix, ρ ranges in $(0, 1]$ because $\max_{k,l \in [K]} |P(k, l)| = 1$; when \mathcal{F} is Normal distribution, ρ ranges in $(0, +\infty)$. For detail, see Examples 1-8.
- For Ω , it is the expectation of A under BiMMDF and we call it population adjacency matrix. Benefitted from the fact that $\text{rank}(\Pi_r) = K, \text{rank}(\Pi_c) = K, \text{rank}(P) = K$ and $K \ll \min(n_r, n_c)$, the rank of Ω is K by Equation (1), i.e., Ω has a low-dimensional structure with only K nonzero singular values. We benefit a lot from Ω 's low-dimensional structure when we design an algorithm to fit BiMMDF in Section 3.
- For \mathcal{F} , it can be any distribution as long as Equation (1) holds. Several distributions are considered in Examples 1-8. It is possible that Equation (1) does not hold for some distributions. For example, \mathcal{F} can not be t -distribution whose mean is 0; \mathcal{F} can not be Cauchy distribution whose mean does not exist.

Table 2 summarizes the comparisons of our BiMMDF with some previous models. In particular, BiMMDF can reduce to some previous models with some conditions.

- When \mathcal{F} is Bernoulli distribution such that $A \in \{0, 1\}^{n_r \times n_c}$, BiMMDF reduces to DiMMSB (Qing & Wang, 2021).
- When \mathcal{F} is Normal or Bernoulli distribution, BiMMDF reduces to the two-way blockmodels (Airoldi et al., 2013).
- When $\Pi_r = \Pi_c, P = P'$, and \mathcal{F} is Bernoulli distribution, BiMMDF reduces to MMSB (Airoldi et al., 2008).

Model	Adjacency matrix A	Distribution \mathcal{F}	Overlapping	Networks can be modeled
SBM Holland et al. (1983)	$A = A'$ and $A \in \{0, 1\}^{n \times n}$	Bernoulli	No	Panel (a) of Figure 1
MMSB Airoldi et al. (2008)	$A = A'$ and $A \in \{0, 1\}^{n \times n}$	Bernoulli	Yes	Panel (a) of Figure 1
DCSBM Karrer & Newman (2011)	$A = A'$ and $A \in \mathbb{N}^{n \times n}$	Bernoulli and Poisson	No	Panel (b) with nonnegative integer weights of Figure 1
OSBM Latouche et al. (2011)	$A = A'$ and $A \in \{0, 1\}^{n \times n}$	Bernoulli	No	Panels (a), (e) of Figure 1
Two-way blockmodels Airoldi et al. (2013)	$A \in \mathbb{R}^{n_r \times n_c}$	Normal and Bernoulli	Yes	Panels (a), (c), (e), (g), (i), (k) of Figure 1
WSBM Aicher et al. (2015)	$A = A', A \in \mathbb{R}^{n \times n}$	Exponential family	No	Panels (a)-(d) of Figure 1
ScBM and DCScBM Rohe et al. (2016)	$A \in \{0, 1\}^{n_r \times n_c}$	Bernoulli	No	Panels (a), (e), (i) of Figure 1
OCCAM Zhang et al. (2020)	$A = A'$ and $A \in \{0, 1\}^{n \times n}$	Bernoulli	Yes	Panel (a) of Figure 1
DCMM Jin et al. (2023)	$A = A'$ and $A \in \{0, 1\}^{n \times n}$	Bernoulli	Yes	Panel (a) of Figure 1
WSBM Palowitch et al. (2017)	$A = A'$ and $A \in \mathbb{R}_+^{n \times n}$	Distributions defined on \mathbb{R}_+	No	Panels (a), (b) of Figure 1
WSBM Ahn et al. (2018)	$A = A'$ and $A \in \mathbb{R}_+^{n \times n}$	Arbitrary	No	Panels (a)-(d) of Figure 1
SBMO Kaufmann et al. (2018)	$A = A'$ and $A \in \{0, 1\}^{n \times n}$	Bernoulli	Yes	Panel (a) of Figure 1
WSBM Xu et al. (2020)	$A = A'$ and $A \in \mathbb{R}_+^{n \times n}$	Arbitrary	No	Panels (a)-(d) of Figure 1
WMMSB Dulac et al. (2020)	$A = A'$ and $A \in \mathbb{N}^{n \times n}$	Poisson	Yes	Panel (b) with nonnegative integer weights of Figure 1
DiMMSB Qing & Wang (2021)	$A \in \{0, 1\}^{n_r \times n_c}$	Bernoulli	Yes	Panels (a), (e), (i) of Figure 1
WSBM Ng & Murphy (2021)	$A = A'$ and $A \in \mathbb{R}_+^{n \times n}$	Gamma	No	Panel (b) of Figure 1
BiDFM and BiDCDFM Qing & Wang (2023)	$A \in \mathbb{R}^{n_r \times n_c}$	Arbitrary	No	Panels (a)-(l) of Figure 1
BiMMDF (this paper)	$A \in \mathbb{R}^{n_r \times n_c}$	Arbitrary	Yes	Panels (a)-(l) of Figure 1

Table 2: Summary of comparisons of BiMMDF with some previous models.

Similar to Mao et al. (2020); Jin et al. (2023), call row node i ‘pure’ if $\Pi_r(i, :)$ degenerates (i.e., one entry is 1, all others $K - 1$ entries are 0) and ‘mixed’ otherwise. The same definitions hold for column nodes. In this article, we assume that for every $k \in [K]$, there exists at least one pure row node i such that $\Pi_r(i, k) = 1$ and at least one pure column node j such that $\Pi_c(j, k) = 1$, and these two assumptions are known as pure node assumption (Mao et al., 2020, 2018; Zhang et al., 2020; Qing & Wang, 2021; Jin et al., 2023). The requirements $\text{rank}(\Pi_r) = K$ and $\text{rank}(\Pi_c) = K$ in Definition 1 hold immediately as long as each row (column) community has at least one pure node. Since we assume that P is full rank and the pure node assumption holds, Proposition 1 of Qing & Wang (2021) guarantees that BiMMDF is identifiable. Meanwhile, the full rank condition on P and pure node assumption on membership matrices are necessary for the identifiability of models for overlapping networks, to name a few, MMSB (Mao et al., 2020), DCMM (Mao et al., 2018; Jin et al., 2023), and OCCAM (Zhang et al., 2020).

3. A spectral algorithm for fitting the model

Since the rank of P is K , we have $\text{rank}(\Omega) = K$. Let $\Omega = U\Lambda V'$ be the top- K singular value decomposition (SVD) of Ω such that $U \in \mathbb{R}^{n_r \times K}$, $\Lambda \in \mathbb{R}_+^{K \times K}$, $V \in \mathbb{R}^{n_c \times K}$, $U'U = I$, $V'V = I$. Lemma 1 of [Qing & Wang \(2021\)](#) which is distribution-free guarantees the existences of simplex structures inherent in U and V , i.e., there exist two $K \times K$ matrices B_r and B_c such that $U = \Pi_r B_r$ and $V = \Pi_c B_c$. Similar to [Mao et al. \(2020\)](#), for simplex structures, applying the successive projection algorithm (SPA) ([Gillis & Vavasis, 2015](#)) to U (and V) with K row (and column) communities obtains B_r (and B_c). Thus, with given Ω , we can exactly return Π_r and Π_c by setting $\Pi_r = UB_r^{-1}$ and $\Pi_c = VB_c^{-1}$.

In practice, Ω is unknown but the adjacency matrix A is given and we aim at estimating Π_r and Π_c based on A . Let $\hat{A} = \hat{U}\hat{\Lambda}\hat{V}'$ be the top- K SVD of A corresponding to the top- K singular values of A where \hat{A} , \hat{U} , $\hat{\Lambda}$, and \hat{V} can be seen as approximations of Ω , U , Λ , and V , respectively. Then one should be able to obtain a good estimation of Π_r (and Π_c) by applying SPA on the rows of \hat{U} (and \hat{V}) assuming there are K row (and column) clusters. The spectral clustering algorithm considered to fit BiMMDF is summarized in Algorithm 1, which is the DiSP algorithm of [Qing & Wang \(2021\)](#) actually. In Algorithm 1, $\hat{\mathcal{I}}_r$ is the index set of pure nodes returned by SPA with input \hat{U} when there are K row communities. Similar explanation holds for $\hat{\mathcal{I}}_c$. Meanwhile, the algorithm for fitting BiMMDF is the same as that of DiMMSB because DiSP enjoys the distribution-free property since Lemma 1 of [Qing & Wang \(2021\)](#) always holds without dependence on distribution \mathcal{F} . Note that there are no tuning parameters required by the DiSP algorithm.

Algorithm 1 DiSP

Require: Adjacency matrix $A \in \mathbb{R}^{n_r \times n_c}$ of a bipartite weighted network \mathcal{N} , number of row (and column) clusters K .

Ensure: $\hat{\Pi}_r$ and $\hat{\Pi}_c$.

- 1: Get the top- K SVD of A as $\hat{U}\hat{\Lambda}\hat{V}'$.
 - 2: $\hat{\mathcal{I}}_r = \text{SPA}(\hat{U})$ and $\hat{\mathcal{I}}_c = \text{SPA}(\hat{V})$.
 - 3: $\hat{B}_r = \hat{U}(\hat{\mathcal{I}}_r, :)$ and $\hat{B}_c = \hat{V}(\hat{\mathcal{I}}_c, :)$.
 - 4: $\hat{Y}_r = \hat{U}\hat{B}_r^{-1}$ and $\hat{Y}_c = \hat{V}\hat{B}_c^{-1}$.
 - 5: $\hat{Y}_r = \max(0, \hat{Y}_r)$ and $\hat{Y}_c = \max(0, \hat{Y}_c)$.
 - 6: $\hat{\Pi}_r = \text{diag}(\hat{Y}_r \mathbf{1}_K)^{-1} \hat{Y}_r$ and $\hat{\Pi}_c = \text{diag}(\hat{Y}_c \mathbf{1}_K)^{-1} \hat{Y}_c$.
-

The time cost of DiSP mainly comes from the SVD step and the SPA step. The SVD step is also known as PCA ([Jin et al., 2023](#)) and it is manageable even for a matrix with a large size. The complexity of SVD is $O(\max(n_r^2, n_c^2)K)$. The time cost of SPA is $O(\max(n_r, n_c)K^2)$ ([Jin et al., 2023](#)). Since the number of clusters K is much smaller than n_r and n_c in this article, as a result, the total time cost of DiSP is $O(\max(n_r^2, n_c^2)K)$. Results in Section 6.4 show that, for a real-world bipartite network with 16726 rows nodes and 22015 column nodes, DiSP takes around 20 seconds to process a standard personal computer (Thinkpad X1 Carbon Gen 8) using MATLAB R2021b.

4. Main results for DiSP

In this section, we show that the sample-based estimates $\hat{\Pi}_r$ and $\hat{\Pi}_c$ concentrate around the true mixed membership matrix Π_r and Π_c , respectively. Throughout this paper, K is a known positive integer.

Set $\tau = \max_{i \in [n_r], j \in [n_c]} |A(i, j) - \Omega(i, j)|$ and $\gamma = \frac{\max_{i \in [n_r], j \in [n_c]} \mathbb{E}[(A(i, j) - \Omega(i, j))^2]}{\rho}$, where τ and γ are two parameters depending on distribution \mathcal{F} . For theoretical convenience, we need the following assumption.

Assumption 1. Assume that $\rho\gamma \max(n_r, n_c) \geq \tau^2 \log(n_r + n_c)$.

Assumption 1 controls the lower bound of $\rho\gamma$ for our theoretical analysis. Because γ varies for different \mathcal{F} and depends on ρ , the exact form of Assumption 1 can be obtained immediately for a specific distribution \mathcal{F} . For detail, see Examples 1-8. Meanwhile, theoretical guarantees for spectral methods studied in ([Lei & Rinaldo, 2015](#); [Jin, 2015](#); [Rohe et al., 2016](#); [Jin et al., 2023](#); [Mao et al., 2020, 2018](#); [Zhou & Amini, 2019](#); [Wang et al., 2020](#)) also need requirements like Assumption 1. Similar to conditions in Corollary 3.1 of [Mao et al. \(2020\)](#), to simplify DiSP's theoretical upper bound, we use the following condition.

Condition 1. $\kappa(P) = O(1)$, $\frac{n_r}{n_c} = O(1)$, $\lambda_K(\Pi_r' \Pi_r) = O(\frac{n_r}{K})$, and $\lambda_K(\Pi_c' \Pi_c) = O(\frac{n_c}{K})$.

In Condition 1, $\kappa(P) = O(1)$ means that P is well-conditioned; $\frac{n_r}{n_c} = O(1)$ means that n_r is in the same order as n_c ; $\lambda_K(\Pi_r^T \Pi_r) = O(\frac{n_r}{K})$ means that the “size” of each row community is in the same order. We are ready to present the main theorem.

Theorem 1. (Error of DiSP) Under $\text{BiMMDF}(n_r, n_c, K, P, \rho, \Pi_r, \Pi_c, \mathcal{F})$, let $\hat{\Pi}_r$ and $\hat{\Pi}_c$ be obtained from Algorithm 1, suppose Assumption 1 and Condition 1 hold, and furthermore, $\sigma_K(\Omega) \gg \sqrt{\rho \gamma (n_r + n_c) \log(n_r + n_c)}$, there exists two permutation matrices $\mathcal{P}_r, \mathcal{P}_c \in \mathbb{R}^{K \times K}$ such that with probability at least $1 - o((n_r + n_c)^{-5})$, for $i \in [n_r], j \in [n_c]$, we have

$$\|e'_i(\hat{\Pi}_r - \Pi_r \mathcal{P}_r)\|_1 = O\left(\frac{K^2 \sqrt{\gamma \log(n_r + n_c)}}{\sigma_K(P) \sqrt{\rho n_c}}\right), \|e'_j(\hat{\Pi}_c - \Pi_c \mathcal{P}_c)\|_1 = O\left(\frac{K^2 \sqrt{\gamma \log(n_r + n_c)}}{\sigma_K(P) \sqrt{\rho n_r}}\right).$$

Epecially, when $n_r = O(n), n_c = O(n)$, we have

$$\|e'_i(\hat{\Pi}_r - \Pi_r \mathcal{P}_r)\|_1 = O\left(\frac{K^2 \sqrt{\gamma \log(n)}}{\sigma_K(P) \sqrt{\rho n}}\right), \|e'_j(\hat{\Pi}_c - \Pi_c \mathcal{P}_c)\|_1 = O\left(\frac{K^2 \sqrt{\gamma \log(n)}}{\sigma_K(P) \sqrt{\rho n}}\right).$$

From Theorem 1, we see that our DiSP enjoys consistent estimation under our BiMMDF, i.e., theoretical upper bounds of DiSP’s error rates go to zero as n_r and n_c go to infinity when P, K, ρ and distribution \mathcal{F} are fixed.

Epecially, under the same settings of Theorem 1, when $n_r = n_c = n, K = O(1)$ (i.e., K is a small positive integer), and n is not too small, Theorem 1 says that DiSP’s error rates are small with high probability when $\sigma_K(P) \gg \sqrt{\frac{\gamma \log(n)}{\rho n}}$. For convenience, we need the following definition for our further analysis.

Definition 2. Let $\text{BiMMDF}(n, 2, \Pi_r, \Pi_c, \alpha_{\text{in}}, \alpha_{\text{out}}, \mathcal{F})$ be a special case of $\text{BiMMDF}(n_r, n_c, K, P, \rho, \Pi_r, \Pi_c, \mathcal{F})$ when $n_r = n_c = n, K = 2$, Condition 1 holds, and ρP has diagonal entries $p_{\text{in}} = \alpha_{\text{in}} \frac{\log(n)}{n}$ and non-diagonal entries $p_{\text{out}} = \alpha_{\text{out}} \frac{\log(n)}{n}$, where $|\alpha_{\text{in}}|$ should not equal to $|\alpha_{\text{out}}|$ because BiMMDF’s identifiability requires P to be full rank.

The following corollary provides conditions on α_{in} and α_{out} to make DiSP’s error rates small with high probability.

Corollary 1. (Separation condition) Under $\text{BiMMDF}(n, 2, \Pi_r, \Pi_c, \alpha_{\text{in}}, \alpha_{\text{out}}, \mathcal{F})$, when n is not too small, with probability at least $1 - o(n^{-5})$, DiSP’s error rates are small and close to zero as long as

$$\gamma \max(|\alpha_{\text{in}}|, |\alpha_{\text{out}}|) \geq \tau^2 + o(1) \text{ and } \|\alpha_{\text{in}} - \alpha_{\text{out}}\| \gg \tau. \quad (2)$$

Remark 2. When the network is undirected, all nodes are pure, each community has an equal size, and \mathcal{F} is Bernoulli distribution, $\text{BiMMDF}(n, 2, \Pi_r, \Pi_c, \alpha_{\text{in}}, \alpha_{\text{out}}, \mathcal{F})$ reduces to the SBM case such that nodes connect with probability p_{in} within clusters and p_{out} across clusters. This special case of SBM has been extensively studied, see (Abbe et al., 2015; Hajek et al., 2016; Abbe, 2017). The main finding in Abbe et al. (2015) says that exact recovery is possible if $|\sqrt{\alpha_{\text{in}}} - \sqrt{\alpha_{\text{out}}}| > \sqrt{2}$ and impossible if $|\sqrt{\alpha_{\text{in}}} - \sqrt{\alpha_{\text{out}}}| < \sqrt{2}$, where exact recovery means recovering the partition correctly with high probability when $n \rightarrow \infty$. Corollary 1 says that DiSP’s error rates are small with high probability as long as Equation (2) holds when A is generated from different distribution \mathcal{F} under $\text{BiMMDF}(n, 2, \Pi_r, \Pi_c, \alpha_{\text{in}}, \alpha_{\text{out}}, \mathcal{F})$. For comparison, exact recovery requires that all nodes are pure, the network is undirected, and \mathcal{F} is Bernoulli distribution while small error rates with high probability considered in this paper allow nodes to be mixed, the network to be bipartite, and \mathcal{F} to be any distribution.

For all pairs (i, j) with $i \in [n_r], j \in [n_c]$, Examples 1-8 provide γ ’s upper bound and show that the explicit form of Equation (2) is different for different distribution \mathcal{F} under BiMMDF.

Example 1. When \mathcal{F} is **Bernoulli distribution** such that $A(i, j) \sim \text{Bernoulli}(\Omega(i, j))$, i.e., $A(i, j) \in \{0, 1\}$. For this case, BiMMDF degenerates to DiMSB for bipartite un-weighted networks. For Bernoulli distribution, P should have nonnegative elements, $\mathbb{E}[A(i, j)] = \Omega(i, j)$ satisfies Equation (1), $\mathbb{P}(A(i, j) = 1) = \Omega(i, j)$, and $\frac{\mathbb{E}[(A(i, j) - \Omega(i, j))^2]}{\rho} = \frac{\Omega(i, j)(1 - \Omega(i, j))}{\rho} \leq \frac{\Omega(i, j)}{\rho} \leq 1$, so we have $\tau \leq 1$ and $\gamma \leq 1$, i.e., τ and γ are finite. Then, Assumption 1 means $\rho \geq \frac{\log(n_r + n_c)}{\max(n_r, n_c)}$, a lower bound requirement on ρ for theoretical analysis. Setting γ as 1 in Theorem 1 obtains theoretical upper bounds of error rates of DiSP and we see that increasing ρ decreases error rates. For $\text{BiMMDF}(n, 2, \Pi_r, \Pi_c, \alpha_{\text{in}}, \alpha_{\text{out}}, \mathcal{F})$, ρP

is a probability matrix when \mathcal{F} is Bernoulli distribution, so ρ ranges in $(0, 1]$ since we require $\max_{k,l} |P(k, l)| = 1$, and α_{in} and α_{out} range in $[0, \frac{n}{\log(n)}]$. Setting $\gamma = 1$ and $\tau = 1$ in Equation (2) gives

$$\max(\alpha_{\text{in}}, \alpha_{\text{out}}) \geq 1 + o(1) \text{ and } |\alpha_{\text{in}} - \alpha_{\text{out}}| \gg 1. \quad (3)$$

Example 2. When \mathcal{F} is **Poisson distribution** such that $A(i, j) \sim \text{Poisson}(\Omega(i, j))$, i.e., $A(i, j) \in \mathbb{N}$. For Poisson distribution, P should have positive elements, $\mathbb{E}[A(i, j)] = \Omega(i, j)$ satisfies Equation (1), $\mathbb{P}(A(i, j) = m) = \frac{\Omega(i, j)^m}{m!} e^{-\Omega(i, j)}$ for any nonnegative integer m and $\mathbb{E}[(A(i, j) - \Omega(i, j))^2] = \Omega(i, j) \leq \rho$, so we have γ is finite and $\gamma \leq 1$. Therefore, for Poisson distribution, Assumption 1 means $\rho \geq \frac{\tau^2 \log(n_r + n_c)}{\max(n_r, n_c)}$. Setting γ as 1 in Theorem 1 when \mathcal{F} is Poisson distribution, we find that increasing ρ decreases error rates. For τ , it is an unknown finite positive integer. Since the mean of Poisson distribution can be any positive value, ρ ranges in $(0, +\infty)$. For BiMMDF($n, 2, \Pi_r, \Pi_c, \alpha_{\text{in}}, \alpha_{\text{out}}, \mathcal{F}$), α_{in} and α_{out} range in $(0, +\infty)$ when \mathcal{F} is Poisson distribution. Setting $\gamma = 1$ in Equation (2) gives

$$\max(\alpha_{\text{in}}, \alpha_{\text{out}}) \geq \tau^2 + o(1) \text{ and } |\alpha_{\text{in}} - \alpha_{\text{out}}| \gg \tau. \quad (4)$$

Example 3. When \mathcal{F} is **Binomial distribution** such that $A(i, j) \sim \text{Binomial}(m, \frac{\Omega(i, j)}{m})$ for any positive integer m , i.e., $A(i, j) \in \{0, 1, 2, \dots, m\}$. For Binomial distribution, all elements of P should be nonnegative, $\mathbb{E}[A(i, j)] = \Omega(i, j)$ satisfies Equation (1), and $\mathbb{E}[(A(i, j) - \Omega(i, j))^2] = m \frac{\Omega(i, j)}{m} (1 - \frac{\Omega(i, j)}{m}) = \Omega(i, j) (1 - \frac{\Omega(i, j)}{m}) \leq \rho$. So, $\tau = m$ and $\gamma \leq 1$. Then, Assumption 1 means $\rho \geq \frac{m^2 \log(n_r + n_c)}{\max(n_r, n_c)}$. Setting γ as 1 in Theorem 1 gets theoretical upper bounds of error rates of DiSP when \mathcal{F} is Binomial distribution and we see that increasing ρ decreases error rates. Meanwhile, since $\frac{\Omega(i, j)}{m}$ is a probability, ρ should be less than m for this case. For BiMMDF($n, 2, \Pi_r, \Pi_c, \alpha_{\text{in}}, \alpha_{\text{out}}, \mathcal{F}$), α_{in} and α_{out} range in $(0, \frac{mn}{\log(n)})$ when \mathcal{F} is Binomial distribution. Setting $\gamma = 1, \tau = m$ in Equation (2) when \mathcal{F} is Binomial distribution, we have

$$\max(\alpha_{\text{in}}, \alpha_{\text{out}}) \geq m^2 + o(1) \text{ and } |\alpha_{\text{in}} - \alpha_{\text{out}}| \gg m. \quad (5)$$

Note that when m is 1, the Binomial distribution reduces to the Bernoulli distribution, and we see that Equation (5) matches Equation (3).

Example 4. When \mathcal{F} is **Normal distribution** such that $A(i, j) \sim \text{Normal}(\Omega(i, j), \sigma_A^2)$, i.e., $A(i, j) \in \mathbb{R}$, where σ_A^2 is the variance term of Normal distribution. For this case, BiMMDF reduces to the two-way blockmodels introduced in Airolidi et al. (2013). For Normal distribution, all elements of P are real values, $\mathbb{E}[A(i, j)] = \Omega(i, j)$ satisfies Equation (1), and $\mathbb{E}[(A(i, j) - \Omega(i, j))^2] = \sigma_A^2$. So, $\gamma = \frac{\sigma_A^2}{\rho}$. For τ , it is an unknown finite value. Then, Assumption 1 means $\frac{\sigma_A^2 \max(n_r, n_c)}{\log(n_r + n_c)} \geq \tau^2$. Setting γ as $\frac{\sigma_A^2}{\rho}$ in Theorem 1, we see that increasing ρ (or decreasing σ_A^2) decreases error rates. Here, ρ ranges in $(0, +\infty)$ because the mean of Normal distribution can be any value. Therefore, for BiMMDF($n, 2, \Pi_r, \Pi_c, \alpha_{\text{in}}, \alpha_{\text{out}}, \mathcal{F}$), α_{in} and α_{out} range in $(-\infty, +\infty)$, and we also have $\rho = \max(|p_{\text{in}}|, |p_{\text{out}}|) = \frac{\log(n)}{n} \max(|\alpha_{\text{in}}|, |\alpha_{\text{out}}|)$. Setting $\gamma = \frac{\sigma_A^2}{\rho} = \frac{\sigma_A^2 n}{\max(|\alpha_{\text{in}}|, |\alpha_{\text{out}}|) \log(n)}$ in Equation (2) gives

$$\frac{\sigma_A^2 n}{\log(n)} \geq \tau^2 + o(1) \text{ and } ||\alpha_{\text{in}}| - |\alpha_{\text{out}}|| \gg \tau. \quad (6)$$

Equation (6) differs a lot from Equations (3)-(5) because α_{in} (and α_{out}) can be negative and there is no requirement on $\max(|\alpha_{\text{in}}|, |\alpha_{\text{out}}|)$ for Normal distribution.

Example 5. When \mathcal{F} is **Exponential distribution** such that $A(i, j) \sim \text{Exponential}(\frac{1}{\Omega(i, j)})$, i.e., $A(i, j) \in \mathbb{R}_+$. For Exponential distribution, all elements of P should be positive, $\mathbb{E}[A(i, j)] = \Omega(i, j)$ satisfies Equation (1), and $\mathbb{E}[(A(i, j) - \Omega(i, j))^2] = \Omega^2(i, j) \leq \rho^2$. So, $\gamma \leq \rho$. For τ , it is an unknown finite value. Then, Assumption 1 means $\rho^2 \geq \frac{\tau^2 \log(n_r + n_c)}{\max(n_r, n_c)}$. When setting γ as ρ in Theorem 1, ρ vanishes in the theoretical bounds, and this suggests that increasing ρ does not influence DiSP's error rates. For this case, ρ ranges in $(0, +\infty)$ because ρP is not a probability matrix. For BiMMDF($n, 2, \Pi_r, \Pi_c, \alpha_{\text{in}}, \alpha_{\text{out}}, \mathcal{F}$), α_{in} and α_{out} range in $(0, +\infty)$ because all elements of P are positive for Exponential distribution. Setting $\gamma = \rho = \max(|p_{\text{in}}|, |p_{\text{out}}|) = \frac{\log(n)}{n} \max(\alpha_{\text{in}}, \alpha_{\text{out}})$ in Equation (2) gives

$$\max(\alpha_{\text{in}}^2, \alpha_{\text{out}}^2) \frac{\log(n)}{n} \geq \tau^2 + o(1) \text{ and } |\alpha_{\text{in}} - \alpha_{\text{out}}| \gg \tau. \quad (7)$$

Equation (7) means that even when the second inequality holds, to make DiSP's error rates be small with high probability, $\max(\alpha_{\text{in}}, \alpha_{\text{out}})$ must be large enough to make the first inequality hold because of the $\frac{\log(n)}{n}$ term.

Example 6. When \mathcal{F} is **Uniform distribution** such that $A(i, j) \sim \text{Uniform}(0, 2\Omega(i, j))$, i.e., $A(i, j) \in (0, 2\rho)$. For Uniform distribution, all elements of P should be nonnegative, $\mathbb{E}[A(i, j)] = \frac{0+2\Omega(i, j)}{2} = \Omega(i, j)$ satisfies Equation (1), τ is no larger than 2ρ , and $\mathbb{E}[(A(i, j) - \Omega(i, j))^2] = \frac{4\Omega^2(i, j)}{12} \leq \frac{\rho^2}{3}$, i.e., $\gamma \leq \frac{\rho}{3}$. Therefore, Assumption 1 means $\rho^2 \geq \frac{3\tau^2 \log(n_r + n_c)}{\max(n_r, n_c)}$. Since ρ vanishes in bounds of error rates when setting γ as $\frac{\rho}{3}$ in Theorem 1, increasing ρ does not influence DiSP's performance. Meanwhile, ρ ranges in $(0, +\infty)$ because $\text{Uniform}(0, 2\Omega(i, j))$ has no upper bound requirement on $\Omega(i, j)$ when it is positive. Therefore, α_{in} and α_{out} range in $[0, +\infty)$ because all elements of P are nonnegative for this case. Setting $\gamma = \rho/3 = \max(|p_{\text{in}}|, |p_{\text{out}}|)/3 = \frac{\log(n)}{3n} \max(\alpha_{\text{in}}, \alpha_{\text{out}})$ in Equation (2) gives

$$\max(\alpha_{\text{in}}^2, \alpha_{\text{out}}^2) \frac{\log(n)}{3n} \geq \tau^2 + o(1) \text{ and } |\alpha_{\text{in}} - \alpha_{\text{out}}| \gg \tau. \quad (8)$$

Example 7. When \mathcal{F} is **Logistic distribution** such that $A(i, j) \sim \text{Logistic}(\Omega(i, j), \beta)$, i.e., $A(i, j) \in \mathbb{R}$, where $\beta > 0$. For Logistic distribution, all elements of P are real values, $\mathbb{E}[A(i, j)] = \Omega(i, j)$ satisfies Equation (1), and $\mathbb{E}[(A(i, j) - \Omega(i, j))^2] = \frac{\pi^2 \beta^2}{3}$, i.e., $\gamma = \frac{\pi^2 \beta^2}{3\rho}$. Therefore, Assumption 1 means $\frac{\pi^2 \beta^2 \max(n_r, n_c)}{3 \log(n_r + n_c)} \geq \tau^2$. Setting γ as $\frac{\pi^2 \beta^2}{3\rho}$ in Theorem 1 obtains theoretical upper bounds of DiSP's error rates, and we find that increasing ρ (or decreasing β) decreases error rates. Meanwhile, ρ ranges in $(0, +\infty)$, and α_{in} (and α_{out}) ranges in $(-\infty, +\infty)$ because the mean of Logistic distribution can be any value. Setting $\gamma = \frac{\pi^2 \beta^2}{3\rho} = \frac{\pi^2 \beta^2}{3 \max(|p_{\text{in}}|, |p_{\text{out}}|)} = \frac{\pi^2 \beta^2 n}{3 \max(|\alpha_{\text{in}}|, |\alpha_{\text{out}}|) \log(n)}$ in Equation (2) gives

$$\frac{\pi^2 \beta^2 n}{3 \log(n)} \geq \tau^2 + o(1) \text{ and } \|\alpha_{\text{in}}\| - \|\alpha_{\text{out}}\| \gg \tau. \quad (9)$$

Example 8. BiMMDF can also generate **bipartite signed networks** by setting $\mathbb{P}(A(i, j) = 1) = \frac{1+\Omega(i, j)}{2}$ and $\mathbb{P}(A(i, j) = -1) = \frac{1-\Omega(i, j)}{2}$, i.e., $A(i, j) \in \{-1, 1\}$. For this case, all elements of P are real values, $\mathbb{E}[A(i, j)] = \Omega(i, j)$ satisfies Equation (1), and $\mathbb{E}[(A(i, j) - \Omega(i, j))^2] = 1 - \Omega^2(i, j) \leq 1$, i.e., $\gamma \leq \frac{1}{\rho}$. For τ , its upper bound is 2. Then Assumption 1 means $\frac{\max(n_r, n_c)}{\log(n_r + n_c)} \geq 4$. Setting γ as $\frac{1}{\rho}$ in Theorem 1, we see that increasing ρ decreases error rates. Meanwhile, ρ ranges in $(0, 1)$ because $\frac{1+\Omega(i, j)}{2}$ and $\frac{1-\Omega(i, j)}{2}$ are probabilities. α_{in} and α_{out} range in $(-\frac{n}{\log(n)}, \frac{n}{\log(n)})$ because all elements of P are real values. Setting $\gamma = \frac{1}{\rho} = \frac{1}{\max(|p_{\text{in}}|, |p_{\text{out}}|)} = \frac{n}{\max(|\alpha_{\text{in}}|, |\alpha_{\text{out}}|) \log(n)}$ and $\tau = 2$ in Equation (2) gives

$$\frac{n}{\log(n)} \geq 4 + o(1) \text{ and } \|\alpha_{\text{in}}\| - \|\alpha_{\text{out}}\| \gg 2. \quad (10)$$

Other choices of \mathcal{F} are also possible as long as Equation (1) holds under distribution \mathcal{F} for our BiMMDF. For example, \mathcal{F} can be Geometric, Laplace, and Gamma distributions in <http://www.stat.rice.edu/~dobelman/courses/texts/dis> (accessed on 9 June 2023), where this link also provides details on probability mass function or probability density function for distributions in Examples 1-7.

5. Missing edge

From Examples 4-8, we see that $A(i, j)$ is always nonzero for any node pair (i, j) when A is generated from our BiMMDF, which suggests that there is always an edge between nodes i and j . However, real-world large-scale networks are usually sparse based on the fact that the total number of edges is usually small compared to the number of nodes [Lei & Rinaldo \(2015\)](#). Similar to [Xu et al. \(2020\)](#), an edge with weight 0 is deemed as a missing edge in this paper. To generate missing edges for bipartite weighted networks from our BiMMDF, we introduce the following strategy.

Let \mathcal{M} be a model for bipartite unweighted networks and let $\mathcal{A} \in \{0, 1\}^{n_r \times n_c}$ be a bi-adjacency matrix generated from \mathcal{M} . \mathcal{M} can be models like ScBM and DCScBM [Rohe et al. \(2016\)](#) as long as \mathcal{A} is the bi-adjacency matrix of a bipartite unweighted network. To model real-world large-scale bipartite weighted networks with missing edges, for $i \in [n_r]$, $j \in [n_c]$, we update $A(i, j)$ by $A(i, j)\mathcal{A}(i, j)$.

In particular, when \mathcal{M} is the bipartite Erdős-Rényi random graph $G(n_r, n_c, p)$ [Erdos et al. \(1960\)](#) such that $\mathbb{P}(\mathcal{A}(i, j) = 1) = p$ and $\mathbb{P}(\mathcal{A}(i, j) = 0) = 1 - p$ for $i \in [n_r], j \in [n_c]$, the number of missing edges in A increases as p decreases. p controls the sparsity of A , and we call p sparsity parameter. In Section 6, we will study p 's influence on DiSP's performance.

Remark 3. This remark provides the difference between the scaling parameter ρ and the sparsity parameter p . Since $\mathbb{P}(A(i, j) = 1) = \Omega(i, j) = \rho \Pi_r(i, :) \Pi_c'(j, :)$ and $\mathbb{P}(A(i, j) = 0) = 1 - \rho \Pi_r(i, :) \Pi_c'(j, :)$ when \mathcal{F} is Bernoulli distribution, ρ controls the number of zeros in A and it also controls network sparsity for this case. However, for distributions in Examples 2-8, p does not control network sparsity anymore. Instead, p always controls network sparsity.

6. Experimental Results

In this section, we present example applications of our method, first to simulated networks and then to real-world networks. For simulated networks, to verify our theoretical analysis in Examples 1-8, we investigate the performance of DiSP to the scaling parameter ρ and the separation parameters α_{in} and α_{out} . We also consider missing edges in our simulations by changing the sparsity parameter p . We will also show the power of DiSP in revealing and understanding the latent community structure of real-world networks by introducing several indices, visualizing $\hat{\Pi}_r$ and $\hat{\Pi}_c$, and depicting the row and column communities detected by DiSP.

6.1. Baseline methods

For simulated networks, we compare DiSP with three overlapping community detection approaches:

- SVM-cone-DCMMSB (SVM-cD for short) ([Mao et al., 2018](#)) and Mixed-SCORE ([Jin et al., 2023](#)) are two algorithms for the DCMM model. The original SVM-cD and Mixed-SCORE are designed to estimate mixed memberships for overlapping undirected networks, to make them function for bipartite networks, we modify them in the following way: First, we use the $K \times K$ singular value matrix $\hat{\Lambda}$ to replace their $K \times K$ eigenvalue matrix. Second, we use \hat{U} (and \hat{V}) to replace their eigenvector matrix to estimate membership matrix Π_r (and Π_c) for row (and column) nodes. SVM-cD does not require any tuning parameters. For Mixed-SCORE, we set the threshold T in [Jin et al. \(2023\)](#) as $\log(n_r + n_c)$ in our experimental studies.
- DiMSC ([Qing, 2023](#)) estimates community memberships for overlapping bipartite un-weighted networks generated from the bipartite version of the DCMM model. DiMSC does not require any tuning parameters.

6.2. Evaluation metric

For simulated networks with known Π_r and Π_c , we use Hamming error ([Jin et al., 2023](#)) and Relative Error ([Mao et al., 2020](#)) to evaluate the performance of the algorithms for overlapping community detection with known Π_r and Π_c . These two criteria for a bipartite network are defined as

$$\text{Hamming Error} = \max\left(\frac{\min_{\mathcal{P} \in \mathcal{S}} \|\hat{\Pi}_r \mathcal{P} - \Pi_r\|_1}{n_r}, \frac{\min_{\mathcal{P} \in \mathcal{S}} \|\hat{\Pi}_c \mathcal{P} - \Pi_c\|_1}{n_c}\right),$$

$$\text{Relative Error} = \max\left(\frac{\min_{\mathcal{P} \in \mathcal{S}} \|\hat{\Pi}_r \mathcal{P} - \Pi_r\|_F}{\|\Pi_r\|_F}, \frac{\min_{\mathcal{P} \in \mathcal{S}} \|\hat{\Pi}_c \mathcal{P} - \Pi_c\|_F}{\|\Pi_c\|_F}\right),$$

where \mathcal{S} is the set of $K \times K$ permutation matrices. In the definition of Hamming Error, $\frac{\min_{\mathcal{P} \in \mathcal{S}} \|\hat{\Pi}_r \mathcal{P} - \Pi_r\|_1}{n_r}$ means the l_1 difference between $\hat{\Pi}_r$ and Π_r , where we consider the permutation of community label in $\hat{\Pi}_r$ since the difference between $\hat{\Pi}_r$ and Π_r should not depend on how we tag each of the K row communities. $\frac{\min_{\mathcal{P} \in \mathcal{S}} \|\hat{\Pi}_r \mathcal{P} - \Pi_r\|_1}{n_r}$ ranges in $[0, 1]$ and it is the smaller the better. $\frac{\min_{\mathcal{P} \in \mathcal{S}} \|\hat{\Pi}_c \mathcal{P} - \Pi_c\|_1}{n_c}$ measures the l_1 difference between $\hat{\Pi}_c$ and Π_c . We let Hamming Error be the maximum of $\frac{\min_{\mathcal{P} \in \mathcal{S}} \|\hat{\Pi}_r \mathcal{P} - \Pi_r\|_1}{n_r}$ and $\frac{\min_{\mathcal{P} \in \mathcal{S}} \|\hat{\Pi}_c \mathcal{P} - \Pi_c\|_1}{n_c}$ to measure the performance of a method over both row and column nodes. Thus, Hamming Error ranges in $[0, 1]$, and smaller is better. Similar arguments hold for the definition of Relative Error except that Relative error measures the l_2 difference between the estimated membership matrix and the ground-truth membership matrix. Relative Error is nonnegative, and smaller is better. We do not use metrics like NMI ([Danon et al., 2005](#); [Bagrow, 2008](#); [Luo et al., 2017](#)), ARI ([Hubert & Arabie, 1985](#); [Luo et al., 2017](#)), and overlapping NMI ([Lancichinetti et al., 2009](#); [Zhang et al., 2020](#)) that require binary overlapping membership vectors ([Mao et al., 2018](#)) because entries of Π_r and Π_c considered in this paper may not be binary.

6.3. Synthetic bipartite weighted networks

In this section, we investigate the sensitivity of DiSP and competing approaches to the scaling parameter ρ and sparsity parameter p when the simulated overlapping bipartite weighted networks are generated from different distribution \mathcal{F} under our BiMMDF model. For simulated networks, we aim at validating our theoretical analysis in Examples 1-8 that DiSP has different behaviors when the scaling parameter ρ is changed under different distributions, and investigating the behavior of DiSP when the sparsity parameter p is changed. We also conduct some simulations by changing α_{in} and α_{out} to show that DiSP achieves the threshold in Equation (2) for different distribution \mathcal{F} under $\text{BiMMDF}(n, 2, \Pi_r, \Pi_c, \alpha_{\text{in}}, \alpha_{\text{out}}, \mathcal{F})$. To facilitate comparisons, we summarize simulations conducted in this paper in Table 3.

Table 3: Simulations conducted in this paper.

Distribution \mathcal{F}	Changing scaling parameter ρ	Changing sparse parameter p	Changing α_{in} and α_{out}
Bernoulli	Simulation 1 (a)	Simulation 1 (b)	Simulations 1 (c) and 1(d)
Poisson	Simulation 2 (a)	Simulation 2 (b)	Simulations 2 (c) and 2(d)
Binomial	Simulation 3 (a)	Simulation 3 (b)	Simulations 3 (c) and 3(d)
Normal	Simulation 4 (a)	Simulation 4 (b)	Simulations 4 (c) and 4(d)
Exponential	Simulation 5 (a)	Simulation 5 (b)	Simulations 5 (c) and 5(d)
Uniform	Simulation 6 (a)	Simulation 6 (b)	Simulations 6 (c) and 6(d)
Logistic	Simulation 7 (a)	Simulation 7 (b)	Simulations 7 (c) and 7(d)
Bipartite signed network	Simulation 8 (a)	Simulation 8 (b)	Simulations 8 (c) and 8(d)

For all simulations in this section, unless specified, the parameters $(n_r, n_c, K, P, \rho, \Pi_r, \Pi_c)$ and distribution \mathcal{F} under BiMMDF are set as follows. Let $K = 2$, each row block own $n_{r,0}$ number of pure nodes where the top $Kn_{r,0}$ row nodes $\{1, 2, \dots, Kn_{r,0}\}$ are pure and the rest row nodes $\{Kn_{r,0} + 1, Kn_{r,0} + 2, \dots, n_r\}$ are mixed with membership $(1/K, 1/K, \dots, 1/K)$. Similarly, let each column block own $n_{c,0}$ number of pure nodes where the top $Kn_{c,0}$ column nodes $\{1, 2, \dots, Kn_{c,0}\}$ are pure and column nodes $\{Kn_{c,0} + 1, Kn_{c,0} + 2, \dots, n_c\}$ are mixed with membership $(1/K, 1/K, \dots, 1/K)$. n_r, n_c , scaling parameter ρ , sparsity parameter p , and distribution \mathcal{F} are set independently for each experiment. For distribution (see, Bernoulli, Poisson, Binomial, Exponential, and Uniform distributions) which needs all elements of P to be nonnegative, we set P as

$$P_1 = \begin{bmatrix} 1 & 0.2 \\ 0.3 & 0.8 \end{bmatrix}.$$

For distribution (see, Normal and Logistic distributions as well as bipartite signed network) which allows P to have negative elements, we set P as

$$P_2 = \begin{bmatrix} 1 & -0.2 \\ 0.3 & -0.8 \end{bmatrix}.$$

Meanwhile, when we consider the case $n_r = n_c = n$ for $\text{BiMMDF}(n, 2, \Pi_r, \Pi_c, \alpha_{\text{in}}, \alpha_{\text{out}}, \mathcal{F})$, we set ρP as

$$\tilde{P} = \begin{bmatrix} \alpha_{\text{in}} & \alpha_{\text{out}} \\ \alpha_{\text{out}} & \alpha_{\text{in}} \end{bmatrix} \frac{\log(n)}{n},$$

where we aim at changing α_{in} and α_{out} to investigate their influences on DiSP's performance and verify Equation (2) for different distribution \mathcal{F} .

Remark 4. The only criteria for choosing the $K \times K$ matrix P is, P should be a full rank asymmetric (or symmetric) matrix, $\max_{k,l \in [K]} |P(k, l)| = 1$, and elements of P are positive or nonnegative or can be negative depending on distribution \mathcal{F} as analyzed in Examples 1-8. The only criteria for setting Π_r and Π_c is, they should satisfy conditions in Definition 1, and there exists at least one pure row (and column) node for each row (and column) community.

To generate a random adjacency matrix A with K row (and column) communities and missing edges from distribution \mathcal{F} under our model BiMMDF, each simulation experiment contains the following steps:

- (a) Set $\Omega = \rho \Pi_r P \Pi_c'$.
 - (b) Let $A(i, j)$ be a random number generated from distribution \mathcal{F} with expectation $\Omega(i, j)$ for $i \in [n_r], j \in [n_c]$.
 - (c) Generate $\mathcal{A} \in \{0, 1\}^{n_r \times n_c}$ from the bipartite Erdős-Rényi random graph $G(n_r, n_c, p)$ such that $\mathbb{P}(\mathcal{A}(i, j) = 1) = p$ and $\mathbb{P}(\mathcal{A}(i, j) = 0) = 1 - p$ for $i \in [n_r], j \in [n_c]$.
 - (d) To generate missing edges in A , update $A(i, j)$ by $A(i, j)\mathcal{A}(i, j)$ for $i \in [n_r], j \in [n_c]$.
 - (e) Apply an overlapping community detection approach to A with K row (and column) communities. Record Hamming Error and Relative Error.
 - (f) Repeat (b)-(e) 50 times, and report the averaged Hamming Error and Relative Error over the 50 repetitions.
- We consider the following simulation setups.

6.3.1. Bernoulli distribution

When $A(i, j) \sim \text{Bernoulli}(\Omega(i, j))$ for $i \in [n_r], j \in [n_c]$, by Example 1 we know that all entries of P should be nonnegative.

Simulation 1 (a): changing ρ . Let $n_r = 200, n_c = 300, n_{r,0} = 50, n_{c,0} = 100$, and $P = P_1$. Let the sparsity parameter p in the bipartite Erdős-Rényi random graph $G(n_r, n_c, p)$ be 0.9, i.e., we consider missing edges here. Since ρ should be set no larger than 1 for the Bernoulli distribution, we let ρ range in $\{0.1, 0.2, 0.3, \dots, 1\}$. The numerical results are displayed in panels (a) and (b) of Figure 2. We see that DiSP performs better as ρ increases and this matches analysis in Example 1. Though SVM-cD, DiMSC, and Mixed-SCORE enjoy competitive performances with DiSP when ρ is small, they perform poorer than DiSP when ρ is larger than 0.6.

Simulation 1 (b): Changing p . All parameters are set the same as Simulation 1 (a) except we let $\rho = 0.8$ and p range in $\{0.1, 0.2, \dots, 1\}$, i.e., we study the influence of the sparsity parameter p on the performances of these four approaches in this simulation. Panels (c) and (d) of Figure 2 show the results. DiSP's error rates decrease when p increases such that the number of missing edges decreases. When p is small, all methods perform similarly. However, when p is large, DiSP performs best.

Simulation 1 (c): changing α_{in} and α_{out} . Let $n = n_r = n_c = 300, n_{r,0} = 50, n_{c,0} = 100, p = 1$, and $\rho P = \tilde{P}$. For Bernoulli distribution, α_{in} and α_{out} should be set in $(0, \frac{n}{\log(n)}]$ by Example 1. For this simulation, we let α_{in} and α_{out} range in $\{1, 2, 3, \dots, 30\}$, where $|\alpha_{\text{in}} - \alpha_{\text{out}}| \geq 1$ when $\alpha_{\text{in}} \neq \alpha_{\text{out}}$. The numerical results are shown in panel (e) of Figure 2. We see that DiSP's error rates are large if $\max(\alpha_{\text{in}}, \alpha_{\text{out}})$ is too small even when $|\alpha_{\text{in}} - \alpha_{\text{out}}| \gg 1$ holds, and DiSP's error rates are small if we increase $\max(\alpha_{\text{in}}, \alpha_{\text{out}})$ when $|\alpha_{\text{in}} - \alpha_{\text{out}}| \gg 1$ holds. These results are consistent with the separation condition on α_{in} and α_{out} provided in Equation (3).

Simulation 1 (d): changing α_{in} and α_{out} . All parameters are set the same as Simulation 1 (c) except that we let α_{in} and α_{out} range in $\{5, 7.5, 10, 12.5, \dots, 50\}$, where $|\alpha_{\text{in}} - \alpha_{\text{out}}| \geq 2.5$ when $\alpha_{\text{in}} \neq \alpha_{\text{out}}$ (note that 2.5 is larger than 1 in Simulation 1 (c)). The numerical results are shown in panel (f) of Figure 2. We see that the "white" area (i.e., large error rates area of α_{in} and α_{out}) is narrower than that of the panel (e). This suggests that when the first inequality of Equation (3) holds, increasing $|\alpha_{\text{in}} - \alpha_{\text{out}}|$ decreases DiSP's error rates. This phenomenon holds naturally because the community detection problem is easier as $|p_{\text{in}} - p_{\text{out}}| = |\alpha_{\text{in}} - \alpha_{\text{out}}| \frac{\log(n)}{n}$ increases.

6.3.2. Poisson distribution

When $A(i, j) \sim \text{Poisson}(\Omega(i, j))$ for $i \in [n_r], j \in [n_c]$, by Example 2, all elements of P should be positive.

Simulation 2 (a): changing ρ . Let $n_r = 200, n_c = 300, n_{r,0} = 50, n_{c,0} = 100, p = 0.9$, and $P = P_1$. Since ρ can be set in $(0, +\infty)$ for Poisson distribution, we let ρ range in $\{0.5, 1, 1.5, \dots, 5\}$. The results are displayed in panels (a) and (b) of Figure 3. We see that increasing ρ decreases DiSP's error rates, and this is consistent with findings in Example 2. In this setting, DiSP has the best performance among all 4 procedures.

Simulation 2 (b): Changing p . All parameters are set the same as Simulation 2 (a) except we let $\rho = 2$ and p range in $\{0.1, 0.2, \dots, 1\}$. The results are reported in panels (c) and (d) of Figure 3, which suggest that DiSP performs better when there are lesser missing edges and DiSP outperforms its competitors when p is larger than 0.6.

Simulation 2 (c): changing α_{in} and α_{out} . Let $n = n_r = n_c = 300, n_{r,0} = 50, n_{c,0} = 100, p = 1$, and $\rho P = \tilde{P}$. α_{out} should be set in $(0, +\infty)$ by Example 2. Here, we let α_{in} and α_{out} be in the range of $\{10, 15, 20, \dots, 100\}$, where $|\alpha_{\text{in}} - \alpha_{\text{out}}| \geq 5$ when $\alpha_{\text{in}} \neq \alpha_{\text{out}}$. The numerical results are shown in panel (e) of Figure 3. The analysis is similar to Simulation 1 (e), and we omit it here.

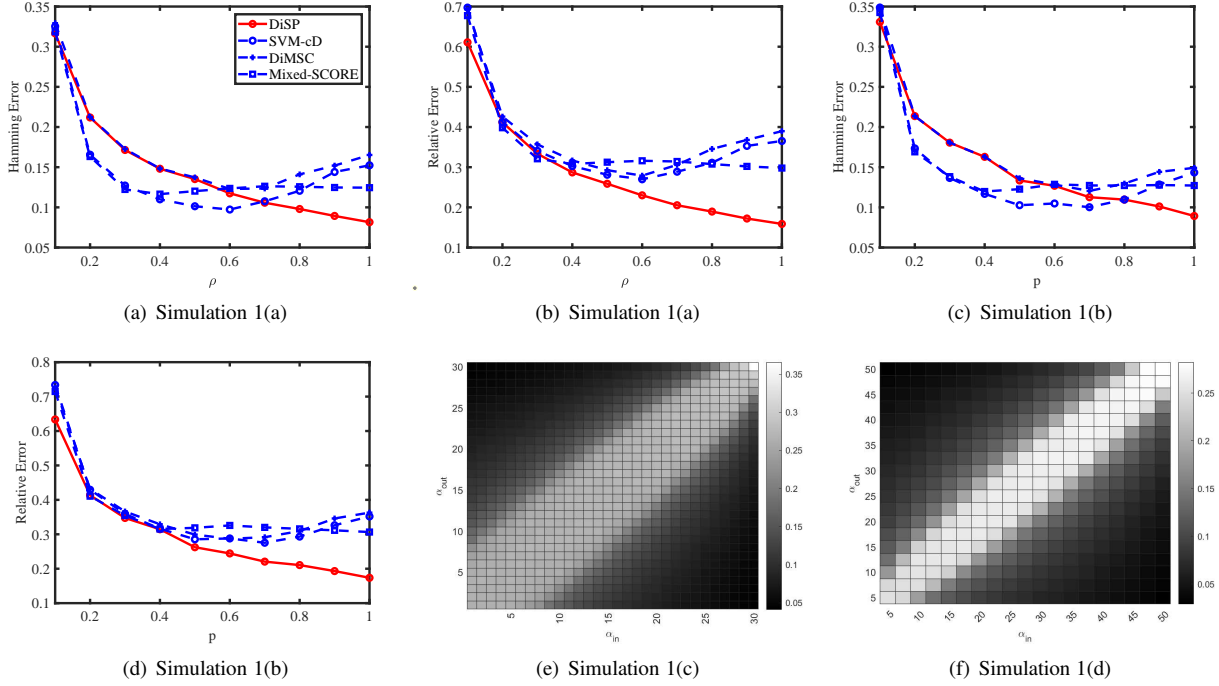


Figure 2: Bernoulli distribution. For panels (e) and (f): the darker pixel represents a lower Hamming Error of DiSP.

Simulation 2 (d): changing α_{in} and α_{out} . All parameters are set the same as Simulation 2 (c) except that we let α_{in} and α_{out} be in the range of $\{200, 300, 400, \dots, 2000\}$ for this simulation, where $|\alpha_{in} - \alpha_{out}| \geq 100$ when $\alpha_{in} \neq \alpha_{out}$. Panel (f) of Figure 3 shows the results. The analysis is similar to Simulation 1 (f), and we omit it here.

6.3.3. Binomial distribution

When $A(i, j) \sim \text{Binomial}(m, \frac{\Omega(i, j)}{m})$ for any positive integer m for $i \in [n_r]$, $j \in [n_c]$, by Example 3, all elements of P should be nonnegative and ρ should be set less than m .

Simulation 3 (a): changing ρ . Let $n_r = 200, n_c = 300, n_{r,0} = 50, n_{c,0} = 100, p = 0.9, P = P_1$, and $m = 7$. Let ρ range in $\{0.2, 0.4, 0.6, \dots, 2\}$. Panels (a) and (b) of Figure 4 display the results, and we see that DiSP's error rates decrease when increasing ρ , which is consistent with the analysis in Example 3. In this experiment, DiSP and its competitors have very similar error rates when ρ is small while DiSP outperforms its competitors when ρ is larger than 1.

Simulation 3 (b): Changing p . All parameters are set the same as Simulation 3 (a) except we let $\rho = 3$ and p range in $\{0.1, 0.2, \dots, 1\}$. The results are shown in panels (c) and (d) of Figure 4. The analysis is similar to Simulation 2 (b), and we omit it here.

Simulation 3 (c): changing α_{in} and α_{out} . Let $n = n_r = n_c = 300, n_{r,0} = 50, n_{c,0} = 100, m = 7, p = 1$, and $\rho P = \tilde{P}$. For Poisson distribution, α_{in} and α_{out} should be set in $(0, \frac{mn}{\log(n)})$ by Example 3. For this simulation, we let α_{in} and α_{out} be in the range of $\{1, 2, 3, \dots, 20\}$, where $|\alpha_{in} - \alpha_{out}| \geq 1$ when $\alpha_{in} \neq \alpha_{out}$. Panel (e) of Figure 4 shows the results. The analysis is similar to Simulation 1 (e), and we omit it here.

Simulation 3 (d): changing α_{in} and α_{out} . All parameters are set the same as Simulation 3(c) except that we let α_{in} and α_{out} be in the range of $\{15, 30, 45, \dots, 300\}$ for this simulation, where $|\alpha_{in} - \alpha_{out}| \geq 15$ when $\alpha_{in} \neq \alpha_{out}$. Panel (f) of Figure 4 shows the results. The analysis is similar to Simulation 1 (f), and we omit it here.

6.3.4. Normal distribution

When $A(i, j) \sim \text{Normal}(\Omega(i, j), \sigma_A^2)$ for some $\sigma_A^2 > 0$ for $i \in [n_r]$, $j \in [n_c]$, by Example 4, all elements of P are real values and ρ can be set in $(0, +\infty)$.

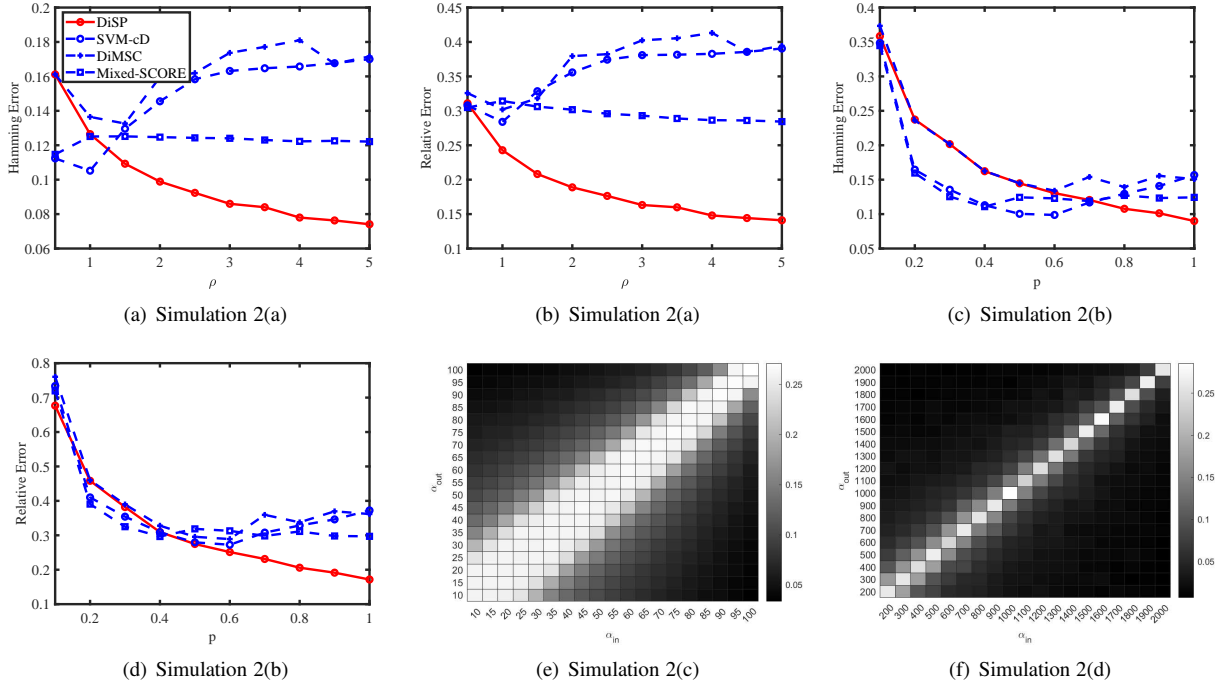


Figure 3: Poisson distribution. For panels (e) and (f): the darker pixel represents a lower Hamming Error.

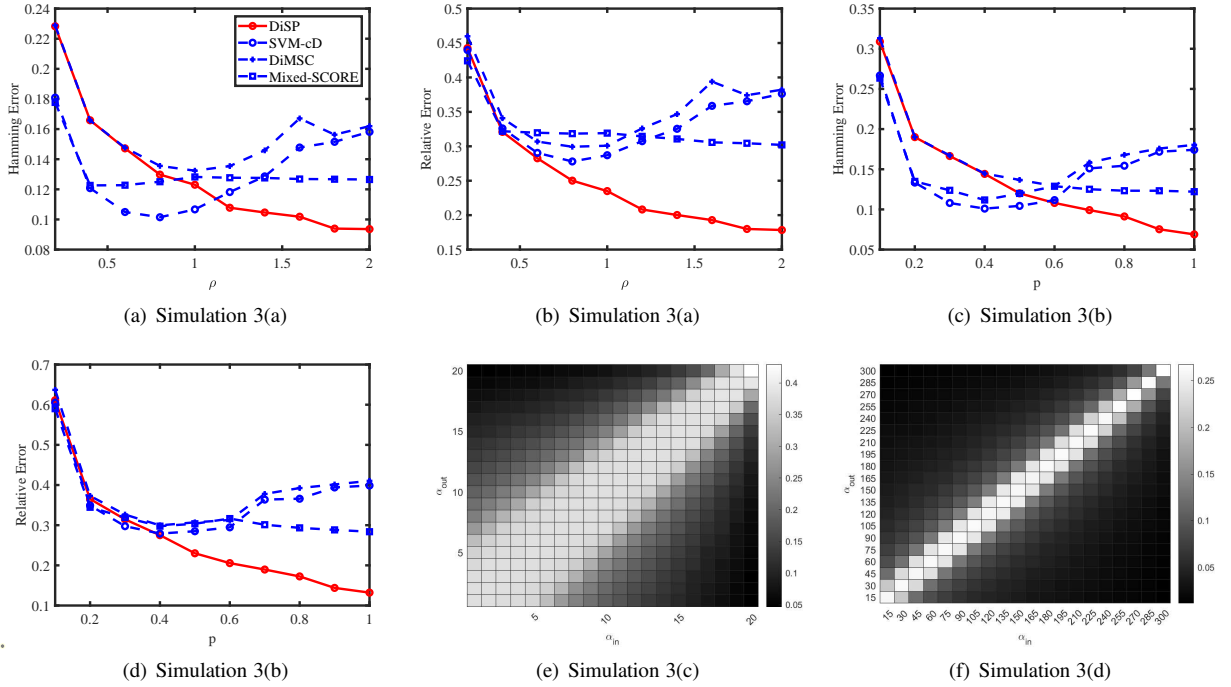


Figure 4: Binomial distribution. For panels (e) and (f): the darker pixel represents a lower Hamming Error.

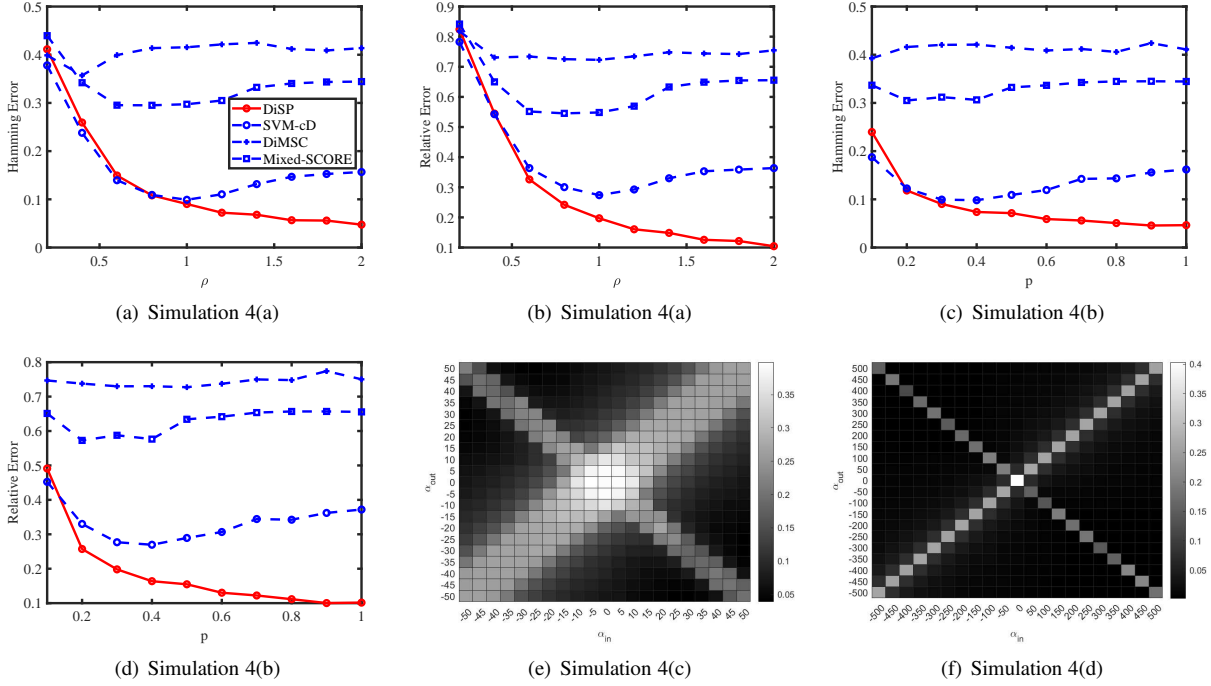


Figure 5: Normal distribution. For panels (e) and (f): the darker pixel represents a lower Hamming Error.

Simulation 4 (a): changing ρ . Let $n_r = 200, n_c = 300, n_{r,0} = 50, n_{c,0} = 100, p = 0.9, P = P_2$, and $\sigma_A^2 = 1$. Let ρ range in $\{0.2, 0.4, 0.6, \dots, 2\}$. The results are shown in panels (a) and (b) of Figure 5. We see that DiSP's error rates decrease when ρ increases and this is consistent with findings in Example 4. When ρ is less than 1, DiSP and SVM-cD have similar error rates, which are smaller than those of DiMSC and Mixed-SCORE. When ρ is larger than 1, DiSP has the best performance among all approaches.

Simulation 4 (b): changing p . All parameters are set the same as Simulation 4 (a) except we let $\rho = 2$ and p range in $\{0.1, 0.2, \dots, 1\}$. The results are displayed in panels (c) and (d) of Figure 5. It suggests that DiSP performs better when p increases and DiSP significantly outperforms its competitors.

Simulation 4 (c): changing α_{in} and α_{out} . Let $n = n_r = n_c = 300, n_{r,0} = 50, n_{c,0} = 100, \sigma_A^2 = 1, p = 1$, and $\rho P = \tilde{P}$. For Normal distribution, α_{in} and α_{out} can be set in $(-\infty, +\infty)$ by Example 4. For this simulation, we let α_{in} and α_{out} be in the range of $\{-50, -45, -40, \dots, 50\}$, where $\|\alpha_{in}\| - \|\alpha_{out}\| \geq 15$ when $|\alpha_{in}| \neq |\alpha_{out}|$. Panel (e) of Figure 5 shows the results. Because the first inequality of Equation (6) does not add a constraint on $\max(|\alpha_{in}|, |\alpha_{out}|)$, DiSP's error rates are small as long as the second inequality holds. We see that results of Simulation 4 (c) support Equation (6) because the “white” area in panel (e) of Figure 5 enjoys a symmetric structure while the “white” areas in panel (e) of Figure 2, panel (e) of Figure 3 and panel (e) of Figure 4 have an asymmetric structure because the first inequality of Equations (3)-(5) has requirement on $\max(\alpha_{in}, \alpha_{out})$.

Simulation 4 (d): changing α_{in} and α_{out} . All parameters are set the same as Simulation 4(c) except that we let α_{in} and α_{out} be in the range of $\{-500, -450, -400, \dots, 500\}$ for this simulation, where $\|\alpha_{in}\| - \|\alpha_{out}\| \geq 150$ when $|\alpha_{in}| \neq |\alpha_{out}|$ (note that 150 is much larger than 15 in Simulation 4 (c)). The results are displayed in panel (f) of Figure 5. Error rates of Simulation 4 (d) are much smaller than that of Simulation 4 (c) because we increase $\|\alpha_{in}\| - \|\alpha_{out}\|$ when $|\alpha_{in}| \neq |\alpha_{out}|$. So, the results of this simulation also support Equation (6).

6.3.5. Exponential distribution

When $A(i, j) \sim \text{Exponential}(\frac{1}{\Omega(i, j)})$ for $i \in [n_r], j \in [n_c]$, by Example 5, P should have positive entries. and ρ can be set in $(0, +\infty)$.

Simulation 5 (a): changing ρ . Let $n_r = 200, n_c = 300, n_{r,0} = 50, n_{c,0} = 100, p = 0.9, P = P_1$. Let ρ range

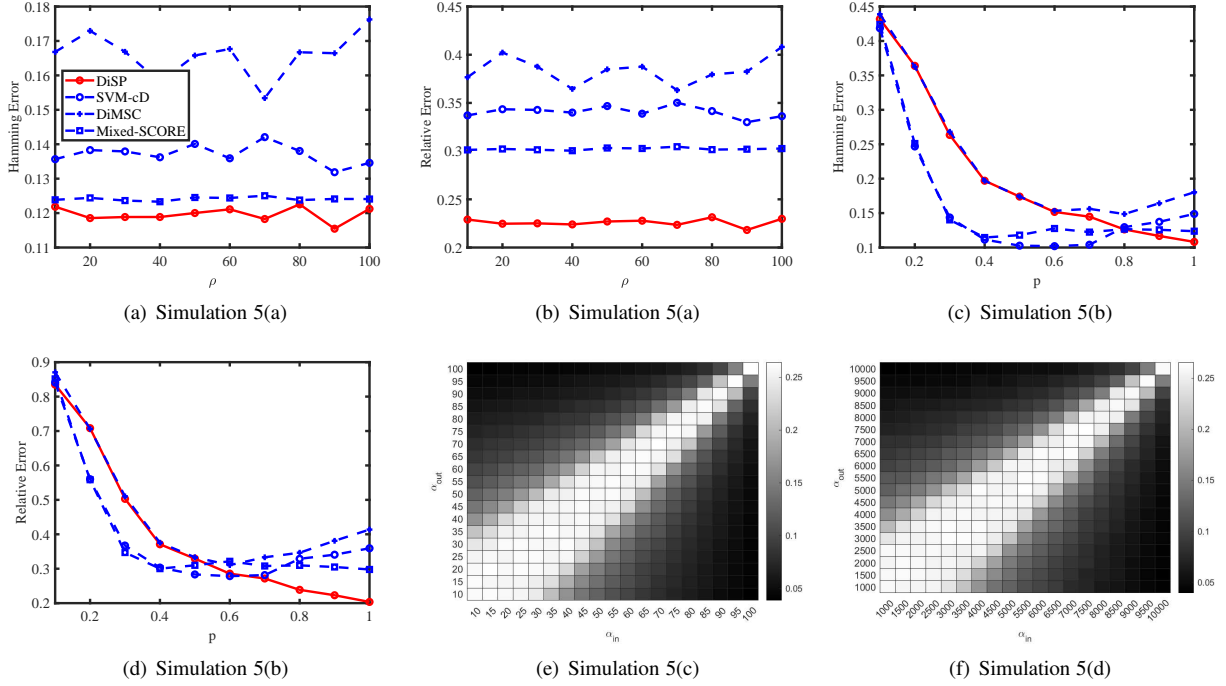


Figure 6: Exponential distribution. For panels (e) and (f): the darker pixel represents a lower Hamming Error.

in $\{10, 20, 30, \dots, 100\}$. In the plot of the result (Figure 6 (a) and (b)), we see that increasing ρ has no influence on DiSP's performance, and this phenomenon matches our findings in Example 5 because ρ vanishes in the theoretical upper bounds of error rates when setting γ as ρ for Exponential distribution. In this experiment, the error rates of DiSP are smaller than that of the best-performing algorithm among the others.

Simulation 5 (b): changing p . All parameters are set the same as Simulation 5 (a) except we let $\rho = 10$ and p range in $\{0.1, 0.2, \dots, 1\}$. The results are shown in panels (c) and (d) of Figure 6. The analysis is similar to Simulation 2 (b), and we omit it here.

Simulation 5 (c): changing α_{in} and α_{out} . Let $n = n_r = n_c = 300, n_{r,0} = 50, n_{c,0} = 100, p = 1$, and $\rho P = \tilde{P}$. For Exponential distribution, α_{in} and α_{out} can be set in $(0, +\infty)$ by Example 5. Here, we let α_{in} and α_{out} be in the range of $\{10, 15, 20, \dots, 100\}$, where $|\alpha_{in} - \alpha_{out}| \geq 5$ when $\alpha_{in} \neq \alpha_{out}$. The numerical results are shown in panel (e) of Figure 6. We see that the “white” area of panel (e) has an asymmetric structure, and this phenomenon occurs because $\max(\alpha_{in}, \alpha_{out})$ should be sufficiently large to make DiSP's error rates small even when the second inequality of Equation (7) holds. We also see that DiSP performs better when increasing $|\alpha_{in} - \alpha_{out}|$.

Simulation 5 (d): changing α_{in} and α_{out} . All parameters are set the same as Simulation 5(c) except that we let α_{in} and α_{out} be in the range of $\{1000, 1500, 2000, \dots, 10000\}$ for this simulation, where $|\alpha_{in} - \alpha_{out}| \geq 500$ when $\alpha_{in} \neq \alpha_{out}$ (note that 500 is much larger than 5 in Simulation 5 (c)). The results are displayed in panel (f) of Figure 6. Unlike Simulations 1-4, the “white” area in panel (f) of Figure 6 still has an asymmetric structure even though 500 is much larger than 5. This phenomenon occurs because the first inequality of Equation (7) is $\max(\alpha_{in}^2, \alpha_{out}^2) \frac{\log(n)}{n} \geq \tau^2 + o(1)$. The $\frac{\log(n)}{n}$ term makes that to make Equation (7) hold, $\max(\alpha_{in}, \alpha_{out})$ must be large enough even when the second inequality of Equation (7) holds. Therefore, the asymmetric structures of “white” areas in panels (e) and (f) of Figure 6 support our findings in Equation (7) for Exponential distribution.

6.3.6. Uniform distribution

When $A(i, j) \sim \text{Uniform}(0, 2\Omega(i, j))$ for $i \in [n_r], j \in [n_c]$, by Example 6, all entries of P should be nonnegative and ρ can be set in $(0, +\infty)$.

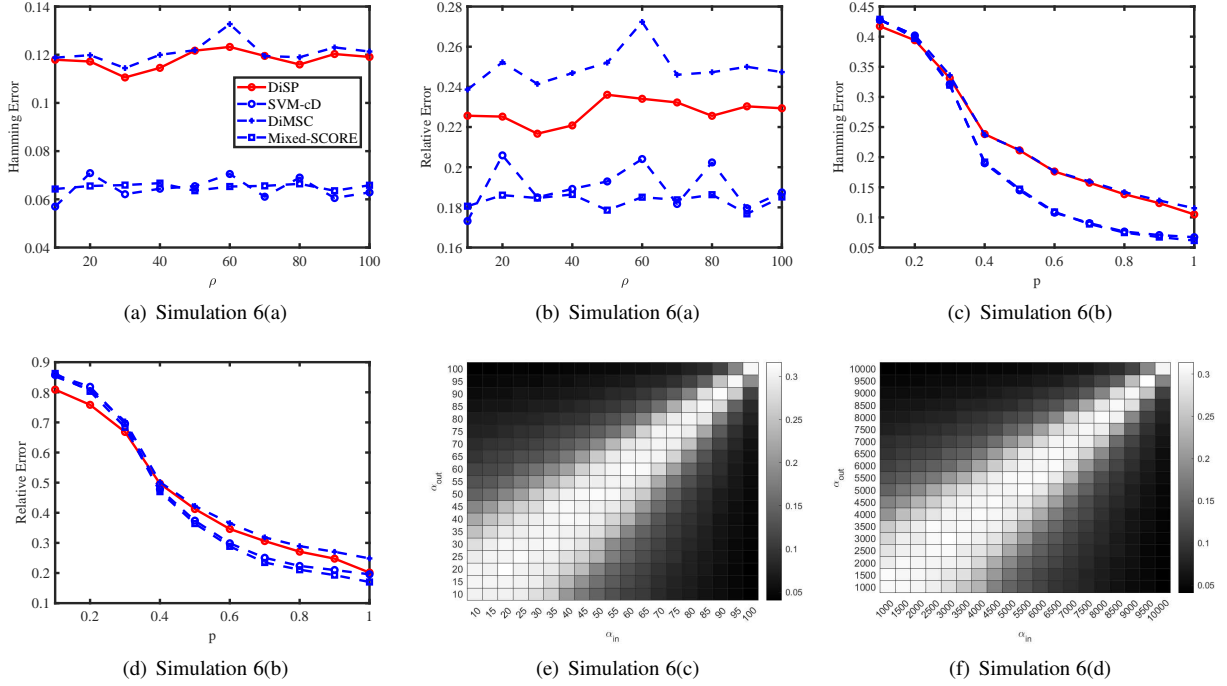


Figure 7: Uniform distribution. For panels (e) and (f): the darker pixel represents a lower Hamming Error.

Simulation 6 (a): changing ρ . Let $n_r = 30, n_c = 50, n_{r,0} = 10, n_{c,0} = 20, p = 0.9, P = P_1$. Let ρ range in $\{10, 20, 30, \dots, 100\}$. Panels (a) and (b) of Figure 7 show the results. We see that ρ has no significant influence on the performances for all 4 algorithms for Uniform distribution, and this verifies our findings in Example 6. In this experiment, though DiSP outperforms DiMSC, it performs slightly poorer than SVM-cD and Mixed-SCORE.

Simulation 6 (b): changing p . All parameters are set the same as Simulation 6 (a) except we let $\rho = 10$ and p range in $\{0.1, 0.2, \dots, 1\}$. The results are displayed in panels (c) and (d) of Figure 7. We see that all procedures have similar error rates and they perform better when there are lesser missing edges as p increases.

Simulation 6 (c): changing α_{in} and α_{out} . Let $n = n_r = n_c = 50, n_{r,0} = 10, n_{c,0} = 20, p = 1$, and $\rho P = \tilde{P}$. For Uniform distribution, α_{in} and α_{out} can be set in $(0, +\infty)$ by Example 6. Here, we let α_{in} and α_{out} be in the range of $\{10, 15, 20, \dots, 100\}$. The numerical results are shown in panel (e) of Figure 7. The analysis for this simulation is similar to that of Simulation 5 (e), and we omit it here.

Simulation 6 (d): changing α_{in} and α_{out} . All parameters are set the same as Simulation 6(c) except that we let α_{in} and α_{out} be in the range of $\{1000, 1500, 2000, \dots, 10000\}$ for this simulation. The numerical results are displayed in the last panel of Figure 7. The analysis is similar to that of Simulation 5 (f), and we omit it here.

6.3.7. Logistic distribution

When $A(i, j) \sim \text{Logistic}(\Omega(i, j), \beta)$ for $\beta > 0$ for $i \in [n_r], j \in [n_c]$, by Example 7, all entries of P are real values and ρ can be set in $(0, +\infty)$.

Simulation 7(a): changing ρ . Let $n_r = 30, n_c = 50, n_{r,0} = 10, n_{c,0} = 20, \beta = 1, p = 0.9$, and $P = P_2$. Let ρ range in $\{0.2, 0.4, 0.6, \dots, 2\}$.

Simulation 7 (b): changing p . All parameters are set the same as Simulation 7 (a) except we let $\rho = 2$ and p range in $\{0.1, 0.2, \dots, 1\}$.

Simulation 7 (c): changing α_{in} and α_{out} . Let $n = n_r = n_c = 50, n_{r,0} = 10, n_{c,0} = 20, \beta = 1, p = 1$, and $\rho P = \tilde{P}$. For Logistic distribution, α_{in} and α_{out} can be set in $(-\infty, +\infty)$ by Example 7. For this simulation, we let α_{in} and α_{out} be in the range of $\{-50, -45, -40, \dots, 50\}$.

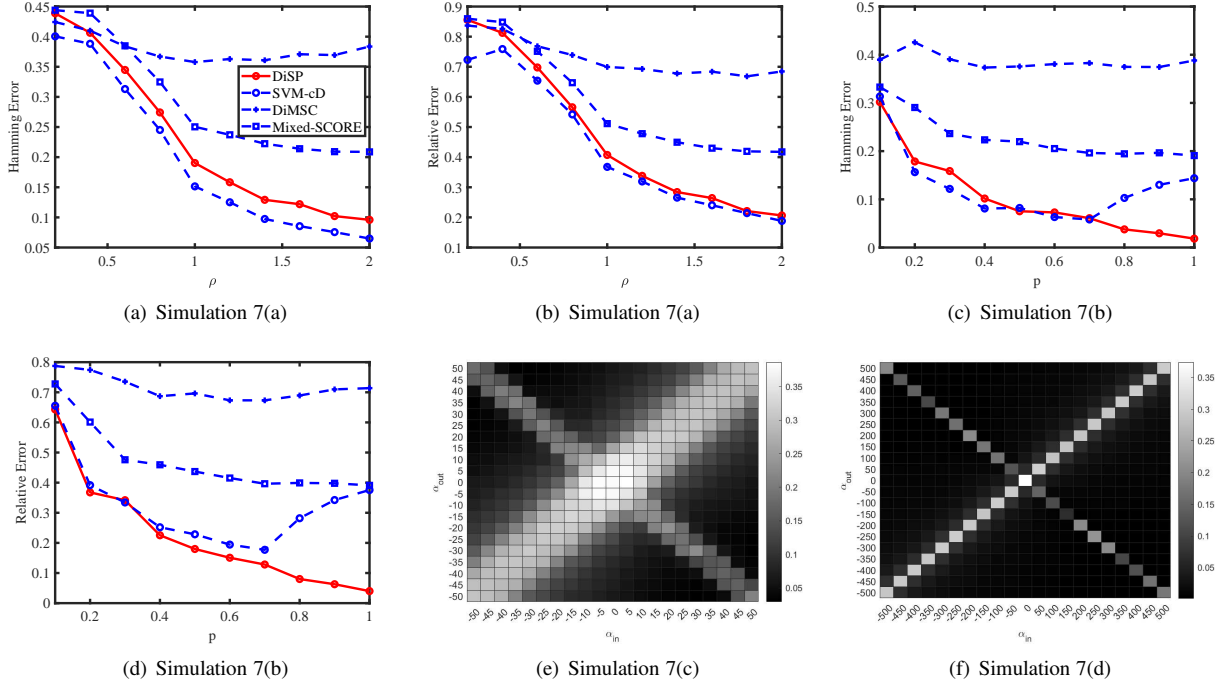


Figure 8: Logistic distribution. For panels (e) and (f): the darker pixel represents a lower Hamming Error.

Simulation 7 (d): changing α_{in} and α_{out} . All parameters are set the same as Simulation 7(c) except that we let α_{in} and α_{out} be in the range of $\{-500, -450, -400, \dots, 500\}$ for this simulation.

Figure 8 displays the results of Simulation 7. The analysis is similar to that of Simulation 4, and we omit it here.

6.3.8. Bipartite signed network

For bipartite signed network when $\mathbb{P}(A(i, j) = 1) = \frac{1+\Omega(i, j)}{2}$ and $\mathbb{P}(A(i, j) = -1) = \frac{1-\Omega(i, j)}{2}$ for $i \in [n_r], j \in [n_c]$, by Example 8, P 's entries are real values and ρ should be set in $(0, 1)$.

Simulation 8 (a): changing ρ . Let $n_r = 100, n_c = 150, n_{r,0} = 30, n_{c,0} = 60, p = 0.9$, and $P = P_2$. Let ρ range in $\{0.1, 0.2, 0.3, \dots, 1\}$.

Simulation 8 (b): changing p . All parameters are set the same as Simulation 8 (a) except we let $\rho = 0.8$ and p range in $\{0.1, 0.2, \dots, 1\}$.

Simulation 8 (c): changing α_{in} and α_{out} . Let $n = n_r = n_c = 300, n_{r,0} = 100, n_{c,0} = 120, p = 1$, and $\rho P = \tilde{P}$. α_{in} and α_{out} can be set in $(-\frac{n}{\log(n)}, \frac{n}{\log(n)})$ by Example 8. For this simulation, we let α_{in} and α_{out} be in the range of $\{-30, -28, -26, \dots, 30\}$.

Simulation 8 (d): changing α_{in} and α_{out} . All parameters are set the same as Simulation 8(c) except that we let α_{in} and α_{out} be in the range of $\{-50, -45, -40, \dots, 50\}$.

Figure 9 displays the results of Simulation 8. The analysis is similar to that of Simulation 4, and we omit it here.

6.3.9. Adjacency matrices with missing edges under different distributions

Simulation 9: For visuality, we plot adjacency matrices of overlapping bipartite weighted networks generated under BiMMDF for different distribution \mathcal{F} . For P , we set it as

$$P_a = \begin{bmatrix} 1 & 0.2 \\ 0.1 & 0.9 \end{bmatrix} \text{ or } P_b = \begin{bmatrix} 1 & -0.2 \\ 0.1 & -0.9 \end{bmatrix}.$$

Under different \mathcal{F} , ρ should be set in the interval obtained in Examples 1-8. We consider below eight settings.

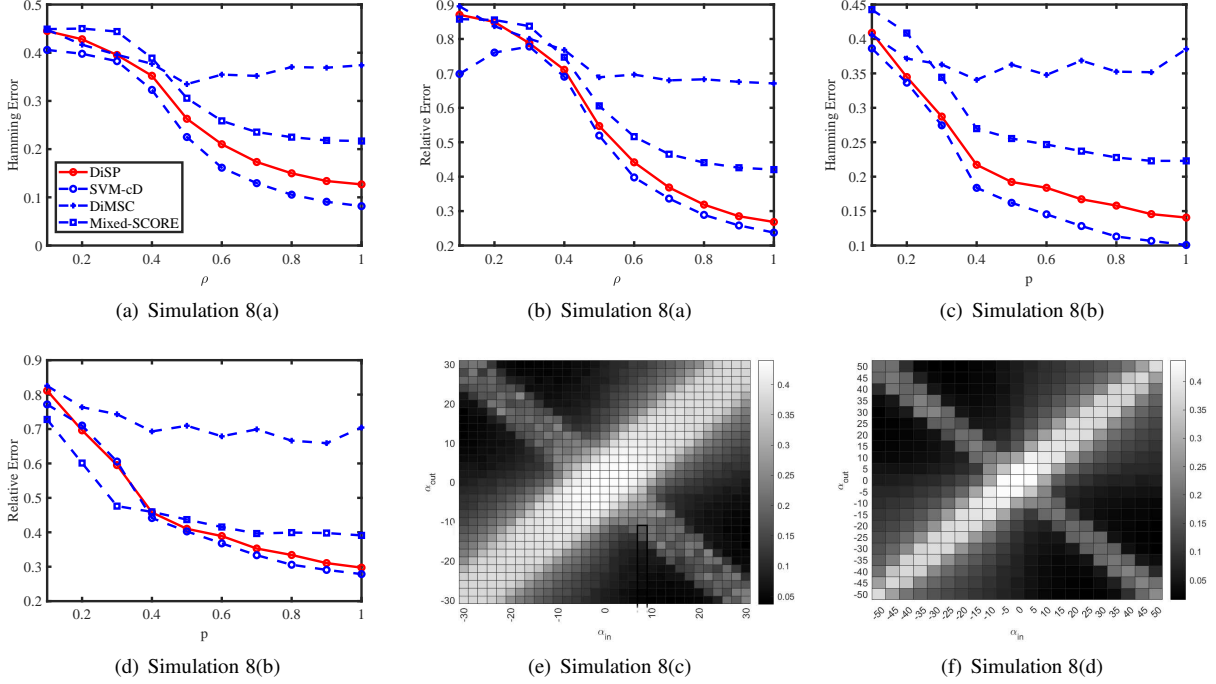


Figure 9: Bipartite signed network. For panels (e) and (f): the darker pixel represents a lower Hamming Error.

Set-up 1: When $A(i, j) \sim \text{Bernoulli}(\Omega(i, j))$ for $i \in [n_r]$, $j \in [n_c]$, set $n_r = 16, n_{r,0} = 7, n_c = 14, n_{c,0} = 6, \rho = 0.9, p = 1$, and $P = P_a$. For this set-up, a bipartite un-weighted network with 16 row nodes and 14 column nodes is generated from BiMMDF. Panel (a) of Figure 10 shows an adjacency matrix A generated from BiMMDF for Set-up 1.

Set-up 2: When $A(i, j) \sim \text{Poisson}(\Omega(i, j))$ for $i \in [n_r]$, $j \in [n_c]$, set $n_r = 16, n_{r,0} = 7, n_c = 14, n_{c,0} = 6, \rho = 60, p = 0.9$, and $P = P_a$. Panel (b) of Figure 10 shows an A generated from BiMMDF for this set-up.

Set-up 3: When $A(i, j) \sim \text{Binomial}(m, \Omega(i, j)/m)$ for $i \in [n_r]$, $j \in [n_c]$, set $n_r = 16, n_{r,0} = 7, n_c = 14, n_{c,0} = 6, m = 7, \rho = 6, p = 0.9$, and $P = P_a$. Panel (c) of Figure 10 shows an A generated from BiMMDF for this set-up.

Set-up 4: When $A(i, j) \sim \text{Normal}(\Omega(i, j), \sigma_A^2)$ for $i \in [n_r]$, $j \in [n_c]$, set $n_r = 10, n_{r,0} = 4, n_c = 8, n_{c,0} = 3, \sigma_A^2 = 1, \rho = 40, p = 0.9$, and $P = P_b$. Panel (d) of Figure 10 shows an A generated from BiMMDF for this set-up.

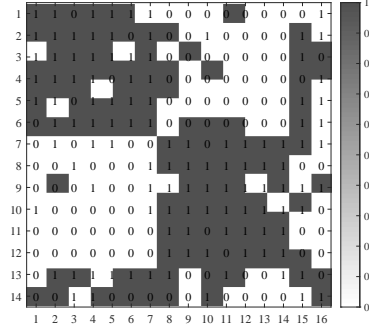
Set-up 5: When $A(i, j) \sim \text{Exponential}(\frac{1}{\Omega(i, j)})$ for $i \in [n_r]$, $j \in [n_c]$, set $n_r = 12, n_{r,0} = 5, n_c = 10, n_{c,0} = 4, \rho = 10, p = 0.9$, and $P = P_a$. Panel (e) of Figure 10 shows an A generated from BiMMDF for this set-up.

Set-up 6: When $A(i, j) \sim \text{Uniform}(0, 2\Omega(i, j))$ for $i \in [n_r]$, $j \in [n_c]$, set $n_r = 10, n_{r,0} = 4, n_c = 8, n_{c,0} = 3, \rho = 10, p = 0.9$, and $P = P_a$. Panel (f) of Figure 10 shows an A generated from BiMMDF for this set-up.

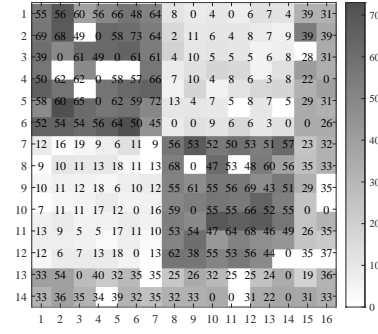
Set-up 7: When $A(i, j) \sim \text{Logistic}(\Omega(i, j), \beta)$ for $i \in [n_r]$, $j \in [n_c]$, set $n_r = 10, n_{r,0} = 4, n_c = 8, n_{c,0} = 3, \beta = 1, \rho = 40, p = 0.9$, and $P = P_b$. Panel (g) of Figure 10 shows an A generated from BiMMDF for this set-up.

Set-up 8: For bipartite signed network when $\mathbb{P}(A(i, j) = 1) = \frac{1+\Omega(i, j)}{2}$ and $\mathbb{P}(A(i, j) = -1) = \frac{1-\Omega(i, j)}{2}$ for $i \in [n_r]$, $j \in [n_c]$, set $n_r = 32, n_{r,0} = 14, n_c = 30, n_{c,0} = 14, \rho = 1, p = 0.9$, and $P = P_b$. Panel (h) of Figure 10 shows an A generated from BiMMDF for this set-up.

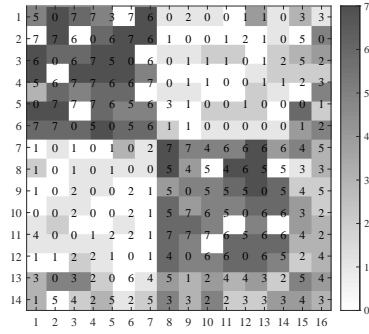
Tables 4 and 5 record Hamming Error and Relative Error of all four approaches for adjacency matrices generated from set-ups 1-8, respectively. The results show that, for set-ups 1, 2, 5, 6, and 7, DiSP outperforms its competitors; for the other three set-ups, DiSP performs similarly to SVM-cD and both methods outperform DiMSC and Mixed-SCORE. With given A and known memberships Π_r and Π_c for these set-ups, readers can apply DiSP to A to check its effectiveness.



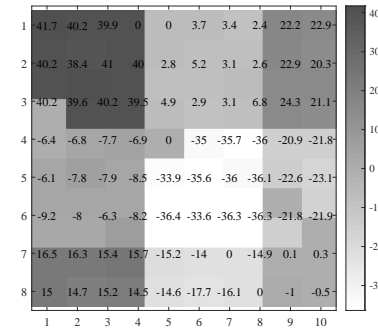
(a) A of Set-up 1



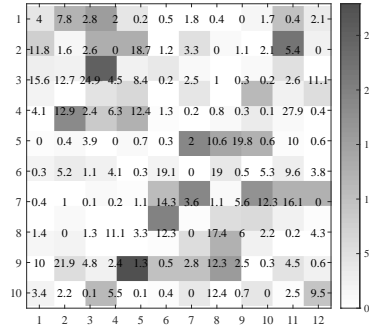
(b) A of Set-up 2



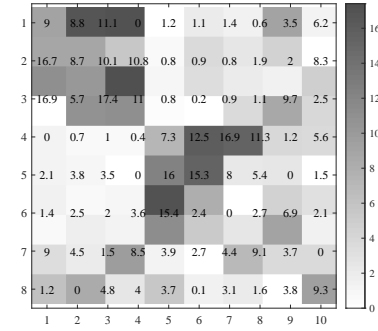
(c) A of Set-up 3



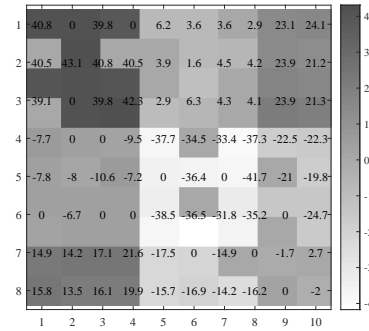
(d) A of Set-up 4



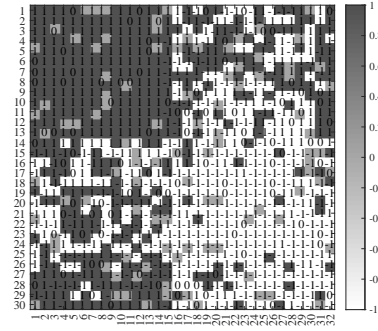
(e) A of Set-up 5



(f) A of Set-up 6



(g) A of Set-up 7



(h) A of Set-up 8

Figure 10: Illustration for bipartite weighted networks' adjacency matrices generated from BiMMDF. In panels (d)-(g), we keep A 's elements in one decimal for visualization beauty. In all panels, some elements of A are zero, suggesting that there are missing edges in A .

Table 4: Hamming Error of methods used in this paper for adjacency matrices generated by Set-ups 1-8.

	Set-up 1	Set-up 2	Set-up 3	Set-up 4	Set-up 5	Set-up 6	Set-up 7	Set-up 8
DiSP	0.0681	0.0295	0.0365	0.0197	0.1490	0.0804	0.0332	0.0774
SVM-cD	0.0710	0.0321	0.0311	0.0169	0.1505	0.0860	0.0358	0.0733
DiMSC	0.1442	0.0704	0.0365	0.3747	0.3379	0.1148	0.3151	0.4010
Mixed-SCORE	0.0734	0.0313	0.0402	0.1906	0.1555	0.0744	0.2213	0.1482

Table 5: Relative Error of methods used in this paper for adjacency matrices generated by Set-ups 1-8.

	Set-up 1	Set-up 2	Set-up 3	Set-up 4	Set-up 5	Set-up 6	Set-up 7	Set-up 8
DiSP	0.2091	0.1030	0.1001	0.0441	0.4632	0.1810	0.0943	0.2225
SVM-cD	0.2142	0.1093	0.0988	0.0507	0.4633	0.2683	0.1060	0.1772
DiMSC	0.4275	0.2310	0.0860	0.7112	0.6743	0.3228	0.5788	0.7298
Mixed-SCORE	0.2038	0.1051	0.1079	0.4076	0.4501	0.2279	0.4327	0.4237

6.4. Real data applications

In addition to the synthetic datasets, we also use DiSP to find community memberships in several real-world networks. Table 6 presents basic information and summarized statistics of real-world networks used in this article. Among these networks, Crisis in a Cloister, Highschool, and Facebook-like Social Network are directed weighted networks whose row nodes are the same as column nodes while the other networks are bipartite. Facebook-like Social Network can be downloaded from https://toreopsahl.com/datasets/#online_social_network (accessed on 9 June 2023) while the other networks can be downloaded from <http://konect.cc/networks> (accessed on 9 June 2023). Since it is meaningless to detect community memberships for isolated nodes which have no connection with any other nodes, we need to remove these isolated nodes before processing data. For Facebook-like Social Network, the original data has 1899 nodes, after removing isolated nodes from both row and column sides, it has 1302 nodes. Unicode languages originally has 614 languages and we remove 86 languages that have not been spoken by the 254 countries. For Marvel, the original data has 19428 works and we remove 6486 works that have no connection with the 6486 characters.

For these networks, their community memberships are unknown and we aim at applying DiSP to have a better understanding of their community structure. For Crisis in a Cloister, K is 3 identified by (Sampson, 1969; Handcock et al., 2007; Airoldi et al., 2008). For networks with unknown K , eigengap is used to estimate it (Rohe et al., 2016). Thus, we plot the top 10 singular values of A in Figure 11 to determine K . For Highschool, Unicode languages, and Marvel, the eigengap suggests $K = 4$. For Facebook-like Social Network, CiaoDVD movie ratings, and arXiv cond-mat, the eigengap suggests $K = 2$. For Amazon (Wang), the eigengap suggests $K = 3$.

Table 6: Basic information and summarized statistics of real-world networks studied in this paper.

	Row node meaning	Column node meaning	Edge meaning	True memberships	n_r	n_c	K	$\max_{i,j} A(i, j)$	$\min_{i,j} A(i, j)$	#Edges
Crisis in a Cloister Sampson (1969)	Monk	Monk	Ratings	Unknown	18	18	3	1	-1	184
Highschool Coleman et al. (1964)	Boy	Boy	Friendship	Unknown	70	70	Unknown	2	0	366
Facebook-like Social Network Opsahl & Panzarasa (2009)	User	User	Messages	Unknown	1302	1302	Unknown	98	0	19044
Unicode languages Kunegis (2013)	Country	Language	Hosts	Unknown	254	528	Unknown	1	0	1106
Marvel Alberich et al. (2002)	Character	Work	Appearance	Unknown	6486	12942	Unknown	1	0	96662
Amazon (Wang) Wang et al. (2010)	User	Item	Rating	Unknown	26112	799	Unknown	5	0	28901
CiaoDVD movie ratings Guo et al. (2014)	User	Movie	Rating	Unknown	17615	16121	Unknown	5	0	72345
arXiv cond-mat Newman (2001b)	Author	Paper	Authorship	Unknown	16726	22015	Unknown	1	0	58595

To explore and understand the community structure of a real-world bipartite (and directed) network, we introduce the following items.

- Let \hat{C}_r be a vector whose i -th element is $\hat{C}_r(i) = \arg\max_{k \in [K]} \hat{\Pi}_r(i, k)$ for $i \in [n_r]$, and we call $\hat{C}_r(i)$ the home base row community of row node i . Define \hat{C}_c by letting $\hat{C}_c(j) = \arg\max_{k \in [K]} \hat{\Pi}_c(j, k)$ for $j \in [n_c]$ and call it home base column community of column node j .
- For row node i , we call it highly mixed row node if $\max_{k \in [K]} \hat{\Pi}_r(i, k) \leq 0.6$ and call it highly pure row node if $\max_{k \in [K]} \hat{\Pi}_r(i, k) \geq 0.9$. A highly mixed (and pure) column node is defined similarly. Note that for row node i whose membership satisfies $0.6 < \max_{k \in [K]} \hat{\Pi}_r(i, k) < 0.9$, it is neither highly mixed nor highly pure.

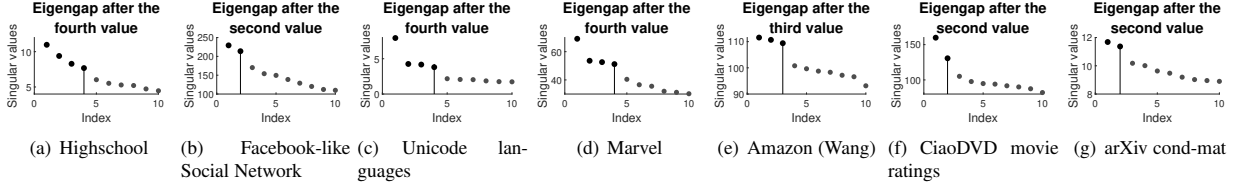


Figure 11: Top 10 singular values of A for seven real-world networks.

- Let $\eta_r = \frac{||\{i: \max_{k \in [K]} \hat{\Pi}_r(i, k) \leq 0.6\}||}{n_r}$ be the proportion of highly mixed row nodes and $\zeta_r = \frac{||\{i: \max_{k \in [K]} \hat{\Pi}_r(i, k) \geq 0.9\}||}{n_r}$ be the proportion of highly pure row nodes. η_c and ζ_c are defined similarly for column nodes.
- For directed networks, we have $n_r = n_c = n$. Since row nodes are the same as column nodes, to measure the asymmetric structure between row communities and column communities, we set $\text{Hamm}_{rc} = \frac{\min_{\mathcal{P} \in \mathcal{S}} ||\hat{\Pi}_r \mathcal{P} - \hat{\Pi}_c||_1}{n}$. Large Hamm_{rc} suggests heavy asymmetric between row and column communities, and vice versa. For undirected networks, Hamm_{rc} is 0, suggesting that Hamm_{rc} is a good way to discover asymmetries in directed networks. Sure, Hamm_{rc} is inapplicable for bipartite networks.

To estimate community memberships of real-world networks in Table 6, we apply DiSP to A with K row (and column) communities, where K is 3 for Crisis in a Cloister, and K used for the other networks is suggested by eigengap in Figure 11. We report $\eta_r, \eta_c, \zeta_r, \zeta_c, \text{Hamm}_{rc}$, and DiSP's runtime in Table 7, where runtime is the average of 10 independent repetitions. From the results on real-world networks, we draw the following conclusions.

- Hamm_{rc} for Crisis in a Cloister and Facebook-like Social Network is larger than that of Highschool. This indicates that the asymmetry between row and column communities for Crisis in a Cloister and Facebook-like Social Network is heavier than that of Highschool.
- Large η_r and η_c for Crisis in a Cloister, Facebook-like Social Network, Marvel, and Amazon (Wang) indicate that there exist large proportions of highly mixed nodes in both row and column communities. For comparison, the other four networks have lesser highly mixed nodes. Meanwhile, Unicode languages, CiaoDVD movie ratings, and arXiv cond-mat have larger proportions of highly pure nodes in both row and column communities than the other networks.
- For Crisis in a Cloister, $18 \times (1 - \eta_r - \zeta_r) \approx 4$ indicates that 4 monks in the row nodes side are neither highly mixed nor highly pure; $18 \times (1 - \eta_c - \zeta_c) \approx 6$ indicates that 6 monks in the column nodes side are neither highly mixed nor highly pure.
- For Highschool, $70 \times (1 - \eta_r - \zeta_r) \approx 31$, i.e., 31 boys in the row nodes side are neither highly mixed nor highly pure; $70 \times (1 - \eta_c - \zeta_c) \approx 33$, i.e., 33 boys in the column nodes side are neither highly mixed nor highly pure.
- For Facebook-like Social Network, most users are neither highly mixed nor highly pure because $1 - \eta_r - \zeta_r = 0.4938$ and $1 - \eta_c - \zeta_c = 0.6252$.
- For Unicode languages, since $\eta_r + \zeta_r = 1$, all countries are either highly mixed or highly pure. Meanwhile, since $\zeta_r = 0.9449$, we see that 94.99% of countries are highly pure, suggesting that nearly 94.99% of countries only belong to one of the four clusters. Since $528 \times \eta_c \approx 43$, we see that only 43 languages are highly mixed while 390 languages are highly pure because $528 \times \zeta_c \approx 390$.
- For Marvel, 81.88% of characters are highly pure and 57.72% of works are neither highly mixed nor highly pure since $1 - \eta_c - \zeta_c = 0.5772$. A similar analysis holds for Amazon (Wang).
- For CiaoDVD movie ratings, all users are either highly mixed or highly pure since $\eta_r + \zeta_r = 1$, 94.43% of users are highly pure, and less than 5% of movies are highly mixed. A similar analysis holds for arXiv cond-mat.

Table 7: $\eta_r, \eta_c, \zeta_r, \zeta_c, \text{Hamm}_{rc}$, and runtime when applying DiSP to real-world networks used in this paper.

data	η_r	η_c	ζ_r	ζ_c	Hamm_{rc}	Runtime
Crisis in a Cloister	0.2222	0.2778	0.5556	0.3889	0.3692	0.0032s
Highschool	0.1429	0.1000	0.4143	0.4286	0.1340	0.0046s
Facebook-like Social Network	0.1951	0.1928	0.3111	0.1820	0.3084	0.0422s
Unicode languages	0.0551	0.0814	0.9449	0.7386	-	0.0117s
Marvel	0.1812	0.2186	0.8188	0.2042	-	3.4237s
Amazon (Wang)	0.3104	0.5156	0.6896	0.2741	-	1.8655s
CiaoDVD movie ratings	0.0557	0.0496	0.9443	0.7153	-	11.0493s
arXiv cond-mat	0.0584	0.0551	0.9416	0.6899	-	20.0398s

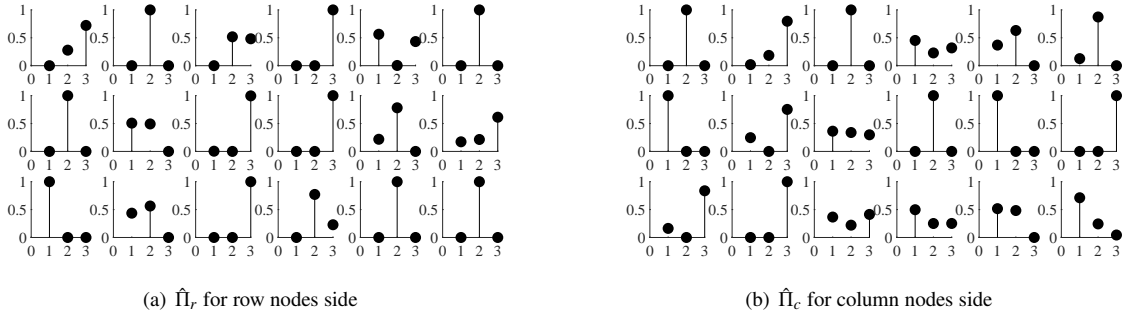


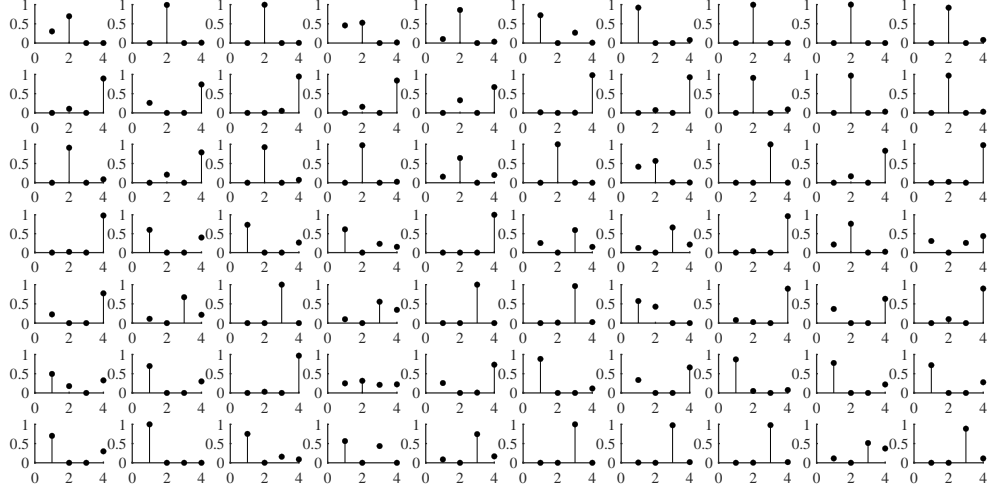
Figure 12: The estimated mixed membership matrices $\hat{\Pi}_r$ and $\hat{\Pi}_c$ detected by DiSP, for the 18 monks in Crisis in a Cloister network. Each sub-panel denotes a membership vector of a monk; we order the communities 1 to 3 on the X axis, and the monk's membership belonging to each cluster is on the Y axis.

For the visualization of community membership of each node, we show the estimated membership matrices $\hat{\Pi}_r$ and $\hat{\Pi}_c$ detected by DiSP for three small scale networks, Crisis in a Cloister, Highschool, and Unicode languages in Figures 12, 13, and 14, respectively. For the visualization of the community structure of both row nodes side and column nodes side, Figure 15 depicts row and column communities identified by DiSP on Crisis in a Cloister and Highschool.

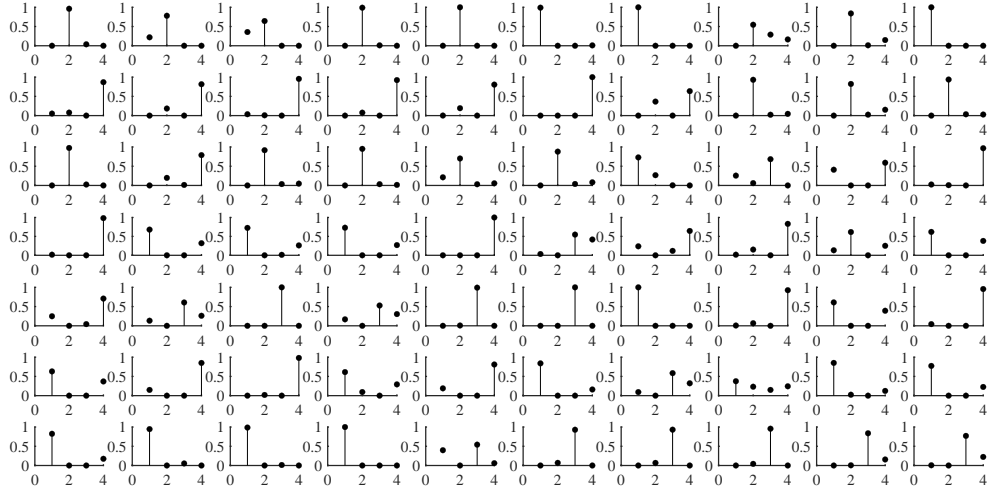
7. Conclusion and future work

In this paper, we investigate the problem of estimating community membership in overlapping bipartite weighted networks. A novel model, named the Bipartite Mixed Membership Distribution-Free (BiMMDF) model, is proposed. An efficient spectral algorithm with a theoretical guarantee of estimation consistency is used to infer the community membership for networks generated from BiMMDF. The separation condition of BiMMDF for different distributions is analyzed in Examples 1-8. We also model large-scale bipartite weighted networks with many missing edges by combining BiMMDF with a model for bipartite un-weighted networks. Our theoretical results are verified by substantial computer-generated bipartite weighted networks. We also apply the algorithm to eight real-world networks with encouraging and interpretable results in understanding community structure of real-world bipartite weighted networks. Our BiMMDF is useful to generate overlapping bipartite weighted networks with true node memberships under different distributions. We expect that BiMMDF will have wide applications in studying the community structure of bipartite weighted networks, just as the mixed membership stochastic blockmodels has been widely studied in recent years.

For future research, first, rigorous methods should be developed to estimate K for overlapping bipartite weighted networks generated from BiMMDF. Actually, more than our BiMMDF, estimating K for all models in Table 2 is a challenging, interesting, and prospective topic. Second, it is possible to design new algorithms based on the ideas of nonnegative matrix factorization or likelihood maximization, or tensor methods mentioned in Mao et al. (2020) to estimate node memberships for networks generated from BiMMDF. Third, like Rohe et al. (2011); Joseph & Yu (2016); Rohe et al. (2016), it is possible to design spectral algorithms based on applications of modified Laplacian matrix

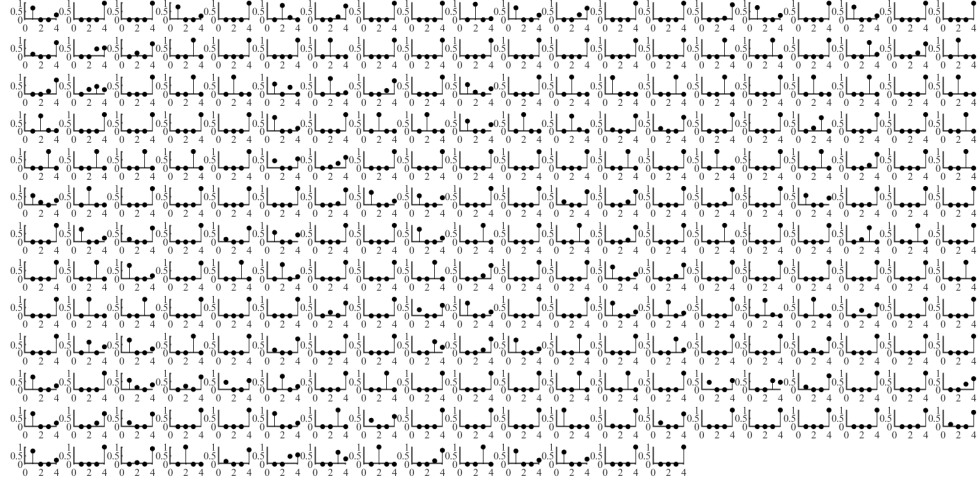


(a) $\hat{\Pi}_r$ for row nodes side

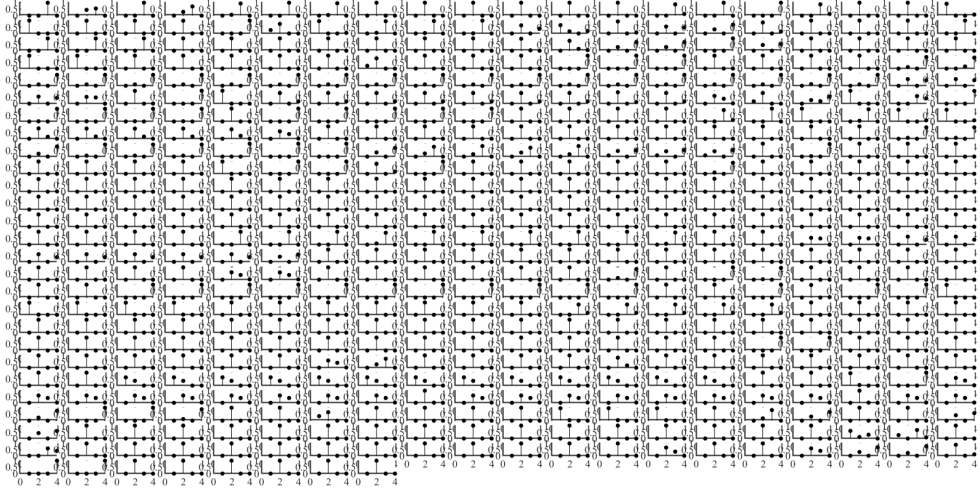


(b) $\hat{\Pi}_c$ for column nodes side

Figure 13: The estimated mixed membership matrices $\hat{\Pi}_r$ and $\hat{\Pi}_c$ detected by DiSP, for the 70 boys in Highschool network. Each sub-panel denotes a membership vector of a boy; we order the communities 1 to 4 on the X axis, and the boy's membership belonging to each cluster is on the Y axis.



(a) $\hat{\Pi}_r$ for row nodes side



(b) $\hat{\Pi}_c$ for column nodes side

Figure 14: The estimated mixed membership matrices $\hat{\Pi}_r$ and $\hat{\Pi}_c$ detected by DiSP for Unicode languages network. For panel (a), each sub-panel denotes a membership vector of a country; for panel (b), each sub-panel denotes a membership vector of a language; we order the communities 1 to 4 on the X axis, and the node's membership belonging to each cluster is on the Y axis.

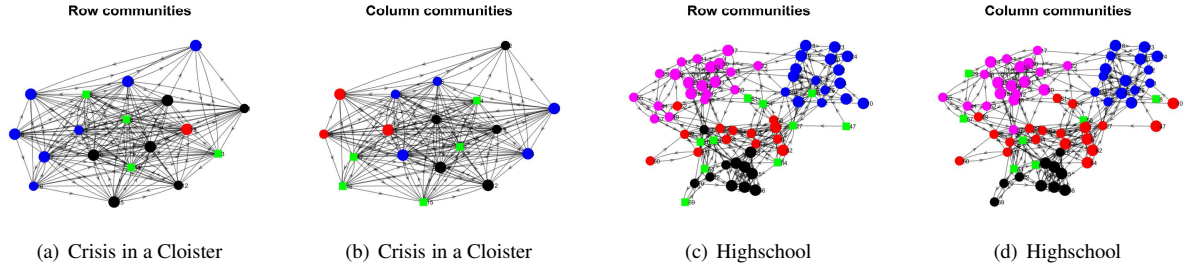


Figure 15: Row and column communities are detected by DiSP for Crisis in a Cloister and Highschool. Colors indicate communities, green square indicate highly mixed nodes and highly pure nodes are enlarged, where the row and column communities are obtained by \hat{C}_r and \hat{C}_c , respectively. For visualization, we do not show edge weights here.

or regularized Laplacian matrix to fit BiMMDF. Forth, DiSP can be accelerated by some random-projection techniques (Zhang et al., 2022) to handle large-scale bipartite weighted networks. Fifth, besides the community structure, identifying the influential nodes to spread information in networks is an appealing topic for researchers. However, BiMMDF can not generate influential nodes in bipartite weighted networks and DiSP only estimates community memberships for overlapping bipartite weighted networks. Thus DiSP can not identify the influential nodes. Though substantial algorithms have been developed to find influential nodes, see algorithms developed in (Zhang et al., 2019; Molaei et al., 2020; Yang & Xiao, 2021; Shang et al., 2021; Boroujeni & Soleimani, 2022; Curado et al., 2023) and references therein, these algorithms only work for un-directed&directed un-weighted&weighted networks with positive edge weights. It is a critical issue to develop algorithms to identify the influential nodes in bipartite weighted networks with negative edge weights. We leave these open problems to future work.

CRediT authorship contribution statement

Huan Qing: Conceptualization, Methodology, Software, Data curation, Writing – original draft, Writing – review & editing. **Jingli Wang:** Data curation, Writing-reviewing & editing, Funding acquisition.

Declaration of competing interest

The authors declare no competing interests.

Data availability

Data and code will be made available on request.

Acknowledgements

Qing’s work was supported by the High level personal project of Jiangsu Province NO.JSSCBS20211218. Wang’s work was supported by the Fundamental Research Funds for the Central Universities, Nankai University, 63221044 and the National Natural Science Foundation of China (Grant 12001295).

References

- Abbe, E. (2017). Community detection and stochastic block models: recent developments. *The Journal of Machine Learning Research*, 18, 6446–6531.
- Abbe, E., Bandeira, A. S., & Hall, G. (2015). Exact recovery in the stochastic block model. *IEEE Transactions on information theory*, 62, 471–487. doi:[10.1109/TIT.2015.2490670](https://doi.org/10.1109/TIT.2015.2490670).
- Ahn, K., Lee, K., & Suh, C. (2018). Hypergraph spectral clustering in the weighted stochastic block model. *IEEE Journal of Selected Topics in Signal Processing*, 12, 959–974. doi:<https://doi.org/10.1109/JSTSP.2018.2837638>.

- Aicher, C., Jacobs, A. Z., & Clauset, A. (2015). Learning latent block structure in weighted networks. *Journal of Complex Networks*, 3, 221–248. doi:<https://doi.org/10.1093/comnet/cnu026>.
- Airoldi, E. M., Blei, D. M., Fienberg, S. E., & Xing, E. P. (2008). Mixed membership stochastic blockmodels. *Journal of Machine Learning Research*, 9, 1981–2014.
- Airoldi, E. M., Wang, X., & Lin, X. (2013). Multi-way blockmodels for analyzing coordinated high-dimensional responses. *The Annals of Applied Statistics*, 7, 2431–2457. doi:<https://doi.org/10.1214/13-AOS643>.
- Alberich, R., Miro-Julia, J., & Rosselló, F. (2002). Marvel universe looks almost like a real social network. *arXiv preprint cond-mat/0202174*, . doi:<https://doi.org/10.48550/arXiv.cond-mat/0202174>.
- Anandkumar, A., Ge, R., Hsu, D., & Kakade, S. (2013). A tensor spectral approach to learning mixed membership community models. In *Conference on Learning Theory* (pp. 867–881). PMLR.
- Bagrow, J. P. (2008). Evaluating local community methods in networks. *Journal of Statistical Mechanics: Theory and Experiment*, 2008, P05001. doi:<https://doi.org/10.1088/1742-5468/2008/05/P05001>.
- Ball, B., Karrer, B., & Newman, M. E. (2011). Efficient and principled method for detecting communities in networks. *Physical Review E*, 84, 036103. doi:<https://doi.org/10.1103/PhysRevE.84.036103>.
- Barabasi, A.-L., & Oltvai, Z. N. (2004). Network biology: understanding the cell's functional organization. *Nature reviews genetics*, 5, 101–113. doi:<https://doi.org/10.1038/nrg1272>.
- Barrat, A., Barthelemy, M., Pastor-Satorras, R., & Vespignani, A. (2004). The architecture of complex weighted networks. *Proceedings of the National Academy of Sciences of the United States of America*, 101, 3747–3752. doi:<https://doi.org/10.1073/pnas.0400087101>.
- Bickel, P. J., & Chen, A. (2009). A nonparametric view of network models and newman–girvan and other modularities. *Proceedings of the National Academy of Sciences*, 106, 21068–21073. doi:<https://doi.org/10.1073/pnas.0907096106>.
- Borgatti, S. P., & Everett, M. G. (1997). Network analysis of 2-mode data. *Social networks*, 19, 243–269. doi:[https://doi.org/10.1016/S0378-8733\(96\)00301-2](https://doi.org/10.1016/S0378-8733(96)00301-2).
- Boroujeni, R. J., & Soleimani, S. (2022). The role of influential nodes and their influence domain in community detection: An approximate method for maximizing modularity. *Expert Systems with Applications*, 202, 117452. doi:<https://doi.org/10.1016/j.eswa.2022.117452>.
- Chen, Y., Chi, Y., Fan, J., Ma, C. et al. (2021). Spectral methods for data science: A statistical perspective. *Foundations and Trends® in Machine Learning*, 14, 566–806. doi:<https://doi.org/10.1561/22000000079>.
- Chen, Y., Li, X., & Xu, J. (2018). Convexified modularity maximization for degree-corrected stochastic block models. *The Annals of Statistics*, 46, 1573–1602. doi:<https://doi.org/10.1214/17-AOS1595>.
- Coleman, J. S. et al. (1964). Introduction to mathematical sociology. *Introduction to mathematical sociology*, .
- Curado, M., Tortosa, L., & Vicent, J. F. (2023). A novel measure to identify influential nodes: return random walk gravity centrality. *Information Sciences*, 628, 177–195. doi:<https://doi.org/10.1016/j.ins.2023.01.097>.
- Danon, L., Diaz-Guilera, A., Duch, J., & Arenas, A. (2005). Comparing community structure identification. *Journal of statistical mechanics: Theory and experiment*, 2005, P09008. doi:<https://doi.org/10.1088/1742-5468/2005/09/P09008>.
- Dulac, A., Gaussier, E., & Langeron, C. (2020). Mixed-membership stochastic block models for weighted networks. In *Conference on Uncertainty in Artificial Intelligence* (pp. 679–688). PMLR.
- Dunne, J. A., Williams, R. J., & Martinez, N. D. (2002). Food-web structure and network theory: The role of connectance and size. *Proceedings of the National Academy of Sciences of the United States of America*, 99, 12917. doi:<https://doi.org/10.1073/pnas.192407699>.
- Erdos, P., Rényi, A. et al. (1960). On the evolution of random graphs. *Publ. Math. Inst. Hung. Acad. Sci.*, 5, 17–60. doi:<https://doi.org/10.1515/9781400841356.38>.
- Fortunato, S. (2010). Community detection in graphs. *Physics reports*, 486, 75–174. doi:<https://doi.org/10.1016/j.physrep.2009.11.002>.
- Fortunato, S., & Hric, D. (2016). Community detection in networks: A user guide. *Physics reports*, 659, 1–44. doi:<https://doi.org/10.1016/j.physrep.2016.09.002>.
- Fortunato, S., & Newman, M. E. (2022). 20 years of network community detection. *Nature Physics*, 18, 848–850. doi:<https://doi.org/10.1038/s41567-022-01716-7>.
- Gillis, N., & Vavasis, S. A. (2015). Semidefinite programming based preconditioning for more robust near-separable nonnegative matrix factorization. *SIAM Journal on Optimization*, 25, 677–698. doi:<https://doi.org/10.1137/130940670>.
- Goldenberg, A., Zheng, A. X., Fienberg, S. E., Airoldi, E. M. et al. (2010). A survey of statistical network models. *Foundations and Trends® in Machine Learning*, 2, 129–233. doi:<https://doi.org/10.1561/22000000005>.
- Gopalan, P., & Blei, D. (2013). Efficient discovery of overlapping communities in massive networks. *Proceedings of the National Academy of Sciences of the United States of America*, 110, 14534–14539. doi:<https://doi.org/10.1073/pnas.1221839110>.
- Guimera, R., & Nunes Amaral, L. A. (2005). Functional cartography of complex metabolic networks. *nature*, 433, 895–900. doi:<https://doi.org/10.1038/nature03288>.
- Guo, G., Zhang, J., Thalmann, D., & Yorke-Smith, N. (2014). Etaf: An extended trust antecedents framework for trust prediction. In *2014 IEEE/ACM International Conference on Advances in Social Networks Analysis and Mining (ASONAM 2014)* (pp. 540–547). IEEE. doi:<https://doi.org/10.1109/ASONAM.2014.6921639>.
- Hajek, B., Wu, Y., & Xu, J. (2016). Achieving exact cluster recovery threshold via semidefinite programming: Extensions. *IEEE Transactions on Information Theory*, 62, 5918–5937. doi:<https://doi.org/10.1109/TIT.2016.2594812>.
- Handcock, M. S., Raftery, A. E., & Tantrum, J. M. (2007). Model-based clustering for social networks. *Journal of the Royal Statistical Society: Series A (Statistics in Society)*, 170, 301–354. doi:<https://doi.org/10.1111/j.1467-985X.2007.00471.x>.
- Holland, P. W., Laskey, K. B., & Leinhardt, S. (1983). Stochastic blockmodels: First steps. *Social Networks*, 5, 109–137. doi:[https://doi.org/10.1016/0378-8733\(83\)90021-7](https://doi.org/10.1016/0378-8733(83)90021-7).
- Hubert, L., & Arabie, P. (1985). Comparing partitions. *Journal of classification*, 2, 193–218. doi:<https://doi.org/10.1007/BF01908075>.
- Javed, M. A., Younis, M. S., Latif, S., Qadir, J., & Baig, A. (2018). Community detection in networks: A multidisciplinary review. *Journal of Network and Computer Applications*, 108, 87–111. doi:<https://doi.org/10.1016/j.jnca.2018.02.011>.
- Jin, D., Yu, Z., Jiao, P., Pan, S., He, D., Wu, J., Yu, P., & Zhang, W. (2021). A survey of community detection approaches: From statistical modeling

- to deep learning. *IEEE Transactions on Knowledge and Data Engineering*, . doi:[10.1109/TKDE.2021.3104155](https://doi.org/10.1109/TKDE.2021.3104155).
- Jin, J. (2015). Fast community detection by SCORE. *Annals of Statistics*, 43, 57–89. doi:<https://doi.org/10.1214/14-AOS1265>.
- Jin, J., Ke, Z. T., & Luo, S. (2023). Mixed membership estimation for social networks. *Journal of Econometrics*, . doi:<https://doi.org/10.1016/j.jeconom.2022.12.003>.
- Joseph, A., & Yu, B. (2016). Impact of regularization on spectral clustering. *The Annals of Statistics*, 44, 1765–1791. doi:<https://doi.org/10.1214/16-AOS1447>.
- Karrer, B., & Newman, M. E. J. (2011). Stochastic blockmodels and community structure in networks. *Physical Review E*, 83, 16107. doi:<https://doi.org/10.1103/PhysRevE.83.016107>.
- Kaufmann, E., Bonald, T., & Lelarge, M. (2018). A spectral algorithm with additive clustering for the recovery of overlapping communities in networks. *Theoretical Computer Science*, 742, 3–26. doi:<https://doi.org/10.1016/j.tcs.2017.12.028>.
- Kunegis, J. (2013). Konect: the koblenz network collection. In *Proceedings of the 22nd international conference on world wide web* (pp. 1343–1350).
- Lancichinetti, A., Fortunato, S., & Kertész, J. (2009). Detecting the overlapping and hierarchical community structure in complex networks. *New journal of physics*, 11, 033015. doi:<https://doi.org/10.1088/1367-2630/11/3/033015>.
- Latapy, M., Magnien, C., & Del Vecchio, N. (2008). Basic notions for the analysis of large two-mode networks. *Social networks*, 30, 31–48. doi:<https://doi.org/10.1016/j.socnet.2007.04.006>.
- Latouche, P., Birmelé, E., & Ambroise, C. (2011). Overlapping stochastic block models with application to the french political blogosphere. *The Annals of Applied Statistics*, 5, 309–336. doi:<https://doi.org/10.1214/10-AOAS382>.
- Le, C. M., Levina, E., & Vershynin, R. (2016). Optimization via low-rank approximation for community detection in networks. *The Annals of Statistics*, 44, 373–400. doi:<https://doi.org/10.1214/15-AOS1360>.
- Lei, J., & Rinaldo, A. (2015). Consistency of spectral clustering in stochastic block models. *Annals of Statistics*, 43, 215–237. doi:<https://doi.org/10.1214/14-AOS1274>.
- Luo, W., Yan, Z., Bu, C., & Zhang, D. (2017). Community detection by fuzzy relations. *IEEE Transactions on Emerging Topics in Computing*, 8, 478–492. doi:<https://doi.org/10.1109/TETC.2017.2751101>.
- Malliaros, F. D., & Vazirgiannis, M. (2013). Clustering and community detection in directed networks: A survey. *Physics reports*, 533, 95–142. doi:<https://doi.org/10.1016/j.physrep.2013.08.002>.
- Mao, X., Sarkar, P., & Chakrabarti, D. (2018). Overlapping clustering models, and one (class) svm to bind them all. In *Advances in Neural Information Processing Systems* (pp. 2126–2136). volume 31.
- Mao, X., Sarkar, P., & Chakrabarti, D. (2020). Estimating mixed memberships with sharp eigenvector deviations. *Journal of the American Statistical Association*, (pp. 1–13). doi:<https://doi.org/10.1080/01621459.2020.1751645>.
- Molaei, S., Farahbakhsh, R., Salehi, M., & Crespi, N. (2020). Identifying influential nodes in heterogeneous networks. *Expert Systems with Applications*, 160, 113580. doi:<https://doi.org/10.1016/j.eswa.2020.113580>.
- Newman, M. E. (2001a). Scientific collaboration networks. i. network construction and fundamental results. *Physical review E*, 64, 016131. doi:<https://doi.org/10.1103/PhysRevE.64.016131>.
- Newman, M. E. (2001b). The structure of scientific collaboration networks. *Proceedings of the national academy of sciences*, 98, 404–409. doi:<https://doi.org/10.1073/pnas.98.2.404>.
- Newman, M. E. (2004). Analysis of weighted networks. *Physical review E*, 70, 056131. doi:<https://doi.org/10.1103/PhysRevE.70.056131>.
- Ng, T. L. J., & Murphy, T. B. (2021). Weighted stochastic block model. *Statistical Methods & Applications*, 30, 1365–1398. doi:<https://doi.org/10.1007/s10260-021-00590-6>.
- Opsahl, T., & Panzarasa, P. (2009). Clustering in weighted networks. *Social networks*, 31, 155–163. doi:<https://doi.org/10.1016/j.socnet.2009.02.002>.
- Palla, G., Barabási, A.-L., & Vicsek, T. (2007). Quantifying social group evolution. *Nature*, 446, 664–667. doi:<https://doi.org/10.1038/nature05670>.
- Palla, G., Derényi, I., Farkas, I., & Vicsek, T. (2005). Uncovering the overlapping community structure of complex networks in nature and society. *nature*, 435, 814–818. doi:<https://doi.org/10.1038/nature03607>.
- Palowitch, J., Bhamidi, S., & Nobel, A. B. (2017). Significance-based community detection in weighted networks. *J. Mach. Learn. Res.*, 18, 188–1.
- Papadopoulos, S., Kompatsiaris, Y., Vakali, A., & Spyridonos, P. (2012). Community detection in social media. *Data mining and knowledge discovery*, 24, 515–554. doi:<https://doi.org/10.1088/1742-5468/2004/10/P10012>.
- Psorakis, I., Roberts, S., Ebdon, M., & Sheldon, B. (2011). Overlapping community detection using bayesian non-negative matrix factorization. *Physical Review E*, 83, 066114. doi:<https://doi.org/10.1103/PhysRevE.83.066114>.
- Qing, H. (2023). Estimating mixed memberships in directed networks by spectral clustering. *Entropy*, 25, 345. doi:<https://doi.org/10.3390/e25020345>.
- Qing, H., & Wang, J. (2021). Directed mixed membership stochastic blockmodel. *arXiv preprint arXiv:2101.02307v3*, . doi:<https://doi.org/10.48550/arXiv.2101.02307>.
- Qing, H., & Wang, J. (2023). Community detection for weighted bipartite networks. *Knowledge-Based Systems*, (p. 110643). doi:<https://doi.org/10.1016/j.knosys.2023.110643>.
- Rohe, K., Chatterjee, S., & Yu, B. (2011). Spectral clustering and the high-dimensional stochastic blockmodel. *The Annals of Statistics*, 39, 1878–1915. doi:<https://doi.org/10.1214/11-AOS887>.
- Rohe, K., Qin, T., & Yu, B. (2016). Co-clustering directed graphs to discover asymmetries and directional communities. *Proceedings of the National Academy of Sciences of the United States of America*, 113, 12679–12684. doi:<https://doi.org/10.1073/pnas.1525793113>.
- Rubinov, M., & Sporns, O. (2010). Complex network measures of brain connectivity: uses and interpretations. *Neuroimage*, 52, 1059–1069. doi:<https://doi.org/10.1016/j.neuroimage.2009.10.003>.
- Sampson, S. F. (1969). *Crisis in a cloister*. Ph.D. thesis Ph. D. Thesis. Cornell University, Ithaca.
- Shang, Q., Deng, Y., & Cheong, K. H. (2021). Identifying influential nodes in complex networks: Effective distance gravity model. *Information*

- Sciences*, 577, 162–179. doi:<https://doi.org/10.1016/j.ins.2021.01.053>.
- Tang, J., Chang, Y., Aggarwal, C., & Liu, H. (2016). A survey of signed network mining in social media. *ACM Computing Surveys (CSUR)*, 49, 1–37. doi:<https://doi.org/10.1145/2956185>.
- Wang, F., Li, T., Wang, X., Zhu, S., & Ding, C. (2011). Community discovery using nonnegative matrix factorization. *Data Mining and Knowledge Discovery*, 22, 493–521. doi:<https://doi.org/10.1007/s10618-010-0181-y>.
- Wang, H., Lu, Y., & Zhai, C. (2010). Latent aspect rating analysis on review text data: a rating regression approach. In *Proceedings of the 16th ACM SIGKDD international conference on Knowledge discovery and data mining* (pp. 783–792). doi:<https://doi.org/10.1145/1835804.1835903>.
- Wang, Z., Liang, Y., & Ji, P. (2020). Spectral algorithms for community detection in directed networks. *Journal of Machine Learning Research*, 21, 1–45.
- Watts, D. J., & Strogatz, S. H. (1998). Collective dynamics of ‘small-world’ networks. *nature*, 393, 440–442. doi:<https://doi.org/10.1038/30918>.
- Xie, J., Kelley, S., & Szymanski, B. K. (2013). Overlapping community detection in networks: The state-of-the-art and comparative study. *Acm computing surveys (csur)*, 45, 1–35. doi:<https://doi.org/10.1145/2501654.2501657>.
- Xu, M., Jog, V., & Loh, P.-L. (2020). Optimal rates for community estimation in the weighted stochastic block model. *Annals of Statistics*, 48, 183–204. doi:<https://doi.org/10.1214/18-AOS1797>.
- Yang, X., & Xiao, F. (2021). An improved gravity model to identify influential nodes in complex networks based on k-shell method. *Knowledge-Based Systems*, 227, 107198. doi:<https://doi.org/10.1016/j.knosys.2021.107198>.
- Zhang, H., Guo, X., & Chang, X. (2022). Randomized spectral clustering in large-scale stochastic block models. *Journal of Computational and Graphical Statistics*, 31, 887–906. doi:<https://doi.org/10.1080/10618600.2022.2034636>.
- Zhang, J., & Wang, J. (2022). Identifiability and parameter estimation of the overlapped stochastic co-block model. *Statistics and Computing*, 32, 57. doi:<https://doi.org/10.1007/s11222-022-10114-1>.
- Zhang, W., Yang, J., Ding, X.-y., Zou, X.-m., Han, H.-y., & Zhao, Q.-c. (2019). Groups make nodes powerful: Identifying influential nodes in social networks based on social conformity theory and community features. *Expert Systems with Applications*, 125, 249–258. doi:<https://doi.org/10.1016/j.eswa.2019.02.007>.
- Zhang, Y., Levina, E., & Zhu, J. (2020). Detecting overlapping communities in networks using spectral methods. *SIAM Journal on Mathematics of Data Science*, 2, 265–283. doi:<https://doi.org/10.1137/19M1272238>.
- Zhao, Y., Levina, E., & Zhu, J. (2012). Consistency of community detection in networks under degree-corrected stochastic block models. *The Annals of Statistics*, 40, 2266–2292. doi:<https://doi.org/10.1214/12-AOS1036>.
- Zhou, Z., & A. Amini, A. (2019). Analysis of spectral clustering algorithms for community detection: the general bipartite setting. *Journal of Machine Learning Research*, 20, 1–47.

Appendix A. Proof of theoretical results for DiSP

Appendix A.1. Proof of Theorem 1

Proof. Let $H_{\hat{U}} = \hat{U}'U$, and $H_{\hat{U}} = U_{H_{\hat{U}}} \Sigma_{H_{\hat{U}}} V_{H_{\hat{U}}}'$ be the top-K SVD of $H_{\hat{U}}$. Define $\text{sgn}(H_{\hat{U}}) = U_{H_{\hat{U}}} V_{H_{\hat{U}}}'$. Let $H_{\hat{V}} = \hat{V}'V$, and $H_{\hat{V}} = U_{H_{\hat{V}}} \Sigma_{H_{\hat{V}}} V_{H_{\hat{V}}}'$ be the top-K SVD of $H_{\hat{V}}$. Define $\text{sgn}(H_{\hat{V}}) = U_{H_{\hat{V}}} V_{H_{\hat{V}}}'$. Based on our model BiMMDF, Assumption 1, and Condition 1, we have below results:

- $\mathbb{E}[A(i, j) - \Omega(i, j)] = 0$ under BiMMDF.
- $\mathbb{E}[(A(i, j) - \Omega(i, j))^2] \leq \rho\gamma$.
- Let $\mu = \max(\frac{n_r \|U\|_{2 \rightarrow \infty}^2}{K}, \frac{n_c \|V\|_{2 \rightarrow \infty}^2}{K})$ be the incoherence parameter defined in Definition 3.1. Chen et al. (2021). By Lemma 8 Qing & Wang (2021) and Condition 1, we have $\mu = O(1)$.
- Let $c_b = \frac{\tau}{\sqrt{\rho \gamma \min(n_r, n_c) (\mu \log(n_r + n_c))}}$. By Condition 1, we have $\min(n_r, n_c) = O(\max(n_r, n_c))$. By the fact that $\mu = O(1)$ given in the last bullet and Assumption 1, we have $c_b \leq O(1)$.
- By $\kappa(P) = O(1)$ in Condition 1 and Lemma 10 Qing & Wang (2021), we have $\kappa(\Omega) = O(1)$.

The first four bullets suggest that the settings and assumptions of Theorem 4.4 Chen et al. (2021) are satisfied, so by Theorem 4.4. Chen et al. (2021), with probability at least $1 - O(\frac{1}{(n_r + n_c)^5})$, we have

$$\max(\|\hat{U} \text{sgn}(H_{\hat{U}}) - U\|_{2 \rightarrow \infty}, \|\hat{V} \text{sgn}(H_{\hat{V}}) - V\|_{2 \rightarrow \infty}) \leq C \frac{\sqrt{\rho \gamma K \log(n_r + n_c)}}{\sigma_K(\Omega)},$$

provided that $\sigma_K(\Omega) \gg \sqrt{\rho \gamma (n_r + n_c) \log(n_r + n_c)}$.

For convenience, let $\varpi = \max(\|\hat{U}\hat{U}' - UU'\|_{2 \rightarrow \infty}, \|\hat{V}\hat{V}' - VV'\|_{2 \rightarrow \infty})$ be the row-wise singular vector error. Since $\|\hat{U}\hat{U}' - UU'\|_{2 \rightarrow \infty} \leq 2\|U - \hat{U}\text{sgn}(H_{\hat{U}})\|_{2 \rightarrow \infty}$ and $\|\hat{V}\hat{V}' - VV'\|_{2 \rightarrow \infty} \leq 2\|V - \hat{V}\text{sgn}(H_{\hat{V}})\|_{2 \rightarrow \infty}$, we have

$$\varpi \leq C \frac{\sqrt{\rho\gamma K \log(n_r + n_c)}}{\sigma_K(\Omega)}.$$

Lemma 10 [Qing & Wang \(2021\)](#) gives $\sigma_K(\Omega) \geq \rho\sigma_K(P)\sigma_K(\Pi_r)\sigma_K(\Pi_c)$, so we have

$$\varpi \leq C \frac{\sqrt{\gamma K \log(n_r + n_c)}}{\sigma_K(P)\sigma_K(\Pi_r)\sigma_K(\Pi_c)\sqrt{\rho}}.$$

By Assumption 1, we have $\sigma_K(\Pi_r) = O(\sqrt{\frac{n_r}{K}})$ and $\sigma_K(\Pi_c) = O(\sqrt{\frac{n_c}{K}})$, which gives

$$\varpi \leq C \frac{K^{1.5} \sqrt{\gamma \log(n_r + n_c)}}{\sigma_K(P) \sqrt{\rho n_r n_c}}. \quad (\text{A.1})$$

By Theorem 2 [Qing & Wang \(2021\)](#) where the proof is distribution-free, there exist two permutation matrices $\mathcal{P}_r, \mathcal{P}_c \in \mathbb{R}^{K \times K}$ such that for $i \in [n_r], j \in [n_c]$,

$$\|e'_i(\hat{\Pi}_r - \Pi_r \mathcal{P}_r)\|_1 = O(\varpi \kappa(\Pi'_r \Pi_r) K \sqrt{\lambda_1(\Pi'_r \Pi_r)}), \|e'_j(\hat{\Pi}_c - \Pi_c \mathcal{P}_c)\|_1 = O(\varpi \kappa(\Pi'_c \Pi_c) K \sqrt{\lambda_1(\Pi'_c \Pi_c)}). \quad (\text{A.2})$$

By Assumption 1 and Equation (A.1), we have

$$\|e'_i(\hat{\Pi}_r - \Pi_r \mathcal{P}_r)\|_1 = O\left(\frac{K^2 \sqrt{\gamma \log(n_r + n_c)}}{\sigma_K(P) \sqrt{\rho n_c}}\right), \|e'_j(\hat{\Pi}_c - \Pi_c \mathcal{P}_c)\|_1 = O\left(\frac{K^2 \sqrt{\gamma \log(n_r + n_c)}}{\sigma_K(P) \sqrt{\rho n_r}}\right).$$

Remark 5. Without Assumption 1, the error bounds of DiSP are always the same as that of Equation (A.2). In this paper, we consider Assumption 1 mainly for theoretical convenience. □

Appendix A.2. Proof of Corollary 1

Proof. For $\text{BiMMDF}(n, 2, \Pi_r, \Pi_c, \alpha_{\text{in}}, \alpha_{\text{out}}, \mathcal{F})$, since $K = 2$, by basic algebra, we have $\sigma_K(\rho P) = \sigma_2(\rho P) = \|p_{\text{in}}\| - \|p_{\text{out}}\| = \rho\sigma_2(P)$. Recall that we let $\max_{k,l \in [K]} |P(k, l)| = 1$ in Definition 1, we have $\max_{k,l \in [K]} |\rho P(k, l)| = \rho = \max(\|p_{\text{in}}\|, \|p_{\text{out}}\|)$, which gives that $\frac{\|p_{\text{in}}\| - \|p_{\text{out}}\|}{\sqrt{\max(\|p_{\text{in}}\|, \|p_{\text{out}}\|)}} = \sqrt{\rho}\sigma_K(P)$ should shrink slower than $\sqrt{\frac{\gamma \log(n)}{n}}$ for small error rates with high probability by Theorem 1. Since $\frac{\|p_{\text{in}}\| - \|p_{\text{out}}\|}{\sqrt{\max(\|p_{\text{in}}\|, \|p_{\text{out}}\|)}} = \frac{\|\alpha_{\text{in}}\| - \|\alpha_{\text{out}}\|}{\sqrt{\max(\|\alpha_{\text{in}}\|, \|\alpha_{\text{out}}\|)}} \sqrt{\frac{\log(n)}{n}}$, $\frac{\|\alpha_{\text{in}}\| - \|\alpha_{\text{out}}\|}{\sqrt{\max(\|\alpha_{\text{in}}\|, \|\alpha_{\text{out}}\|)}}$ should shrink slower than $\sqrt{\gamma}$ for small error rates with high probability, i.e.,

$$\frac{\|\alpha_{\text{in}}\| - \|\alpha_{\text{out}}\|}{\sqrt{\max(\|\alpha_{\text{in}}\|, \|\alpha_{\text{out}}\|)}} \gg \sqrt{\gamma}. \quad (\text{A.3})$$

Meanwhile, since $\rho = \max(\|p_{\text{in}}\|, \|p_{\text{out}}\|) = \frac{\log(n)}{n} \max(\|\alpha_{\text{in}}\|, \|\alpha_{\text{out}}\|)$ under $\text{BiMMDF}(n, 2, \Pi_r, \Pi_c, \alpha_{\text{in}}, \alpha_{\text{out}}, \mathcal{F})$, we have $\frac{\log(n)}{n} \max(\|\alpha_{\text{in}}\|, \|\alpha_{\text{out}}\|) \gamma n \geq \tau^2 \log(2n)$ by Assumption 1, which gives

$$\gamma \max(\|\alpha_{\text{in}}\|, \|\alpha_{\text{out}}\|) \geq \tau^2 \frac{\log(2n)}{\log(n)}. \quad (\text{A.4})$$

Now, when Equation (A.4) holds, Equation (A.3) can be released as

$$\|\alpha_{\text{in}}\| - \|\alpha_{\text{out}}\| \gg \tau \sqrt{\frac{\log(2n)}{\log(n)}}. \quad (\text{A.5})$$

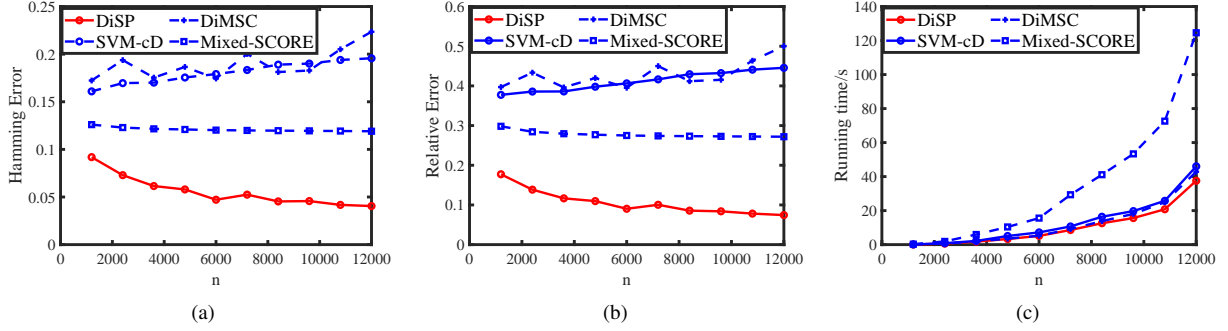


Figure B.16: Panel (a): Hamming Error against increasing n . Panel (b): Relative Error against increasing n . Panel (c): Running time against increasing n .

Since $\frac{\log(2n)}{\log(n)} = \frac{\log(2)}{\log(n)} + 1 = 1 + o(1)$ when n is not too small, Equations (A.4) and (A.5) can be released as

$$\gamma \max(|\alpha_{\text{in}}|, |\alpha_{\text{out}}|) \geq \tau^2 + o(1) \text{ and } \|\alpha_{\text{in}}\| - \|\alpha_{\text{out}}\| \gg \tau. \quad (\text{A.6})$$

Next, we show that the lower bound requirement of $\sigma_K(\Omega)$ in Theorem 1 and $\kappa(P) = O(1)$ in Condition 1 hold naturally as long as Equation (A.6) holds. By Lemma 10 Qing & Wang (2021), we know that $\sigma_2(\Omega) \geq \rho \sigma_2(P) \sigma_2(\Pi_r) \sigma_2(\Pi_c)$ holds under $\text{BiMMDF}(n, 2, \Pi_r, \Pi_c, \alpha_{\text{in}}, \alpha_{\text{out}}, \mathcal{F})$ without other assumptions. Therefore, to guarantee that the condition $\sigma_2(\Omega) \gg \sqrt{\rho \gamma n \log(2n)}$ in Theorem 1 always holds when $n_r = n_c = n$ and $K = 2$ under $\text{BiMMDF}(n, 2, \Pi_r, \Pi_c, \alpha_{\text{in}}, \alpha_{\text{out}}, \mathcal{F})$, we need $\rho \sigma_2(P) \sigma_2(\Pi_r) \sigma_2(\Pi_c) \gg \sqrt{\rho \gamma n \log(2n)} = \sqrt{\rho \gamma n (\log(2) + \log(n))} = O(\sqrt{\rho \gamma n \log(n)})$, i.e.,

$$\sigma_2(P) \gg \sqrt{\frac{\gamma n \log(n)}{\rho \lambda_2(\Pi_r' \Pi_r) \lambda_2(\Pi_c' \Pi_c)}}. \quad (\text{A.7})$$

Since $\lambda_2(\Pi_r' \Pi_r) = O(\frac{n}{2}) = O(n)$, $\lambda_2(\Pi_c' \Pi_c) = O(\frac{n}{2}) = O(n)$ under $\text{BiMMDF}(n, 2, \Pi_r, \Pi_c, \alpha_{\text{in}}, \alpha_{\text{out}}, \mathcal{F})$, Equation (A.7) gives that $\sigma_2(P)$ should shrink slower than $\sqrt{\frac{\gamma \log(n)}{\rho n}}$, which matches with the consistency requirement on $\sigma_2(P)$ obtained from Theorem 1 under $\text{BiMMDF}(n, 2, \Pi_r, \Pi_c, \alpha_{\text{in}}, \alpha_{\text{out}}, \mathcal{F})$. Therefore, under $\text{BiMMDF}(n, 2, \Pi_r, \Pi_c, \alpha_{\text{in}}, \alpha_{\text{out}}, \mathcal{F})$, the lower bound requirement on $\sigma_K(\Omega)$ in Theorem 1 holds naturally as long as Equation (A.6) holds. Finally, since $\kappa(P) = \kappa(\rho P) = \frac{\|\alpha_{\text{in}}\| + \|\alpha_{\text{out}}\|}{\|\alpha_{\text{in}}\| - \|\alpha_{\text{out}}\|}$, we see that $\kappa(P) = O(1)$ in Condition 1 holds immediately when Equation (A.6) holds. \square

Appendix B. Extra simulation results

Changing n : When $n_r = n_c = n$, we record the running time for each approach when n increases. For simplicity, we only consider Normal distribution here. Let $K = 2, \rho = 1, p = 0.9, \sigma_A^2 = 1, n_{r,0} = n/4, n_{c,0} = n/3$, and all mixed nodes have mixed membership $(1/2, 1/2)$. Set the connectivity matrix P as P_2 in Section 6.3. We vary n in the range $\{1200, 2400, \dots, 12000\}$. We report the averaged Hamming Error, the averaged Relative Error, and the averaged running time over 50 repetitions for each n for each method. We see in Figure B.16 that DiSP outperforms its competitors both in estimation errors and running time. Meanwhile, for a bipartite weighted network with 12000 row nodes and 12000 column nodes, DiSP takes around 40 seconds to process a standard personal computer (Thinkpad X1 Carbon Gen 8) using MATLAB R2021b.